



Norwegian University of
Science and Technology

3D Scanning of Corroded Mooring Chain

Alexander Hoel

Master of Science in Mechanical Engineering

Submission date: July 2016

Supervisor: Jochen Kohler, KT

Co-supervisor: Per Jahn Haagensen, KT

Norwegian University of Science and Technology
Department of Structural Engineering



MASTER'S THESIS 2016

SUBJECT AREA: 3D scanning, steel structures	DATE: 15 July 2016	NO. OF PAGES: 16 + 80 + 13
--	-----------------------	-------------------------------

TITLE:

3D Scanning of Corroded Mooring Chain

BY:

Alexander Hoel



SUMMARY:

This thesis is concerned with mooring line failure and 3D representations of corroded chain surfaces. Equipment for making such representations have been evaluated through a feasibility study carried out at NTNU.

An ATOS III sensor was used to measure heavily corroded chain surfaces. Measuring procedures have been evaluated and best practice has been suggested. The produced output was a dense point cloud, mapping an area of approximately 15 500 mm².

The point cloud was post processed in Geomagic Studio 14 and ANSYS ICEM CFD. A surface model processed for inspection routines, was created. Also a model representing a block with a single cavity was made. This was compatible with the software Abaqus.

A submodeling analysis was carried out in Abaqus, to simulate a cavity on the surface of a chain link in static tension. Good conformity was found in the stress response of the edge regions. It was concluded that the submodel was able to recreate the conditions in a chain link surface. Consistency in the location of the critical area of the model was observed. Convergence of the maximum principle stress in the critical area was not proven. The smoothing routine and insufficient minimum size of the elements in the mesh was pointed out as the most plausible explanations.

The use of submodeling analysis in further study is highlighted as a good method for evaluating worst case scenarios considering cavities on the surface of chain links. Advices considering efficiently evaluation of convergence and mesh requirements have been given.

A literature study with main focus on mooring system components and mooring line failure was presented. The historical development considering mooring line failure during the last 20 years was illustrated through statistical data.

RESPONSIBLE TEACHER:	Professor Jochen Köhler
SUPERVISORS:	Professor Jochen Köhler, Professor Per Jahn Haagensen
CARRIED OUT AT:	The Departement of Structural Engineering, NTNU



MASTEROPPGAVE 2016

FAGOMRÅDE: 3D skanning, stål strukturer	DATO: 15.Juli. 2016	ANTALL SIDER: 16 + 80 + 13
--	------------------------	-------------------------------

TITTEL:

3D Skanning av Korrodert Forankringskjetting

UTFØRT AV:

Alexander Hoel



SAMMENDRAG :

Denne avhandlingen tar for seg brudd i forankringslinjer 3D-representasjon av korroderte kjetting overflater. Utstyr som er kapabelt til å lage slike representasjoner har blitt evaluert gjennom en mulighetsstudie utført ved NTNU.

En ATOS III sensor ble brukt til å gjøre målinger korroderte kjetting overflater. Korroderte produksjonsledd ble skannet og målt, målemetoder evaluert. Målemetoder ble vurdert beste fremgangsmåte ble foreslått. Resultatet kom i form av en punkttsky med en stor mengde målepunkter som kartla et område på ca. 15 500 mm².

Punkttskyen ble etterbehandlet i Geomagic Studio 14 og ANSYS ICEM CFD. En overflate modell, tilpasset inspeksjonsrutiner ble produsert. Også en modell som representerte en enkel korrosjons grop ble produsert. Denne var kompatibel med softwaren Abaqus.

En analyse av en submodell ble utført i Abaqus, for å simulere en korrosjons grop på overflaten av en kjetting i statisk strekk. God overensstemmelse av resultater, ble funnet i ytterkantene av modellen. Det ble konkludert med at modellen var i stand til å gjenskape de samme grensebetingelsene som i en kjetting overflate. Modellens kritiske område ble lokalisert i på samme lokasjon i alle analysene. Konvergens av maksimal prinsipiell spenning ble ikke bevist. Glatte funksjonen og utilfredsstillende minimum størrelse på elementene i meshet, ble utpekt som de mest sannsynlige årsakene.

Bruk av analyser med submodeller i videre studier er poengtert som en god metode for å vurdere verst tenkelige scenarier når det kommer til korrosjonsgroper på kjetting overflater. Råd angående effektiv vurdering av konvergens og krav til mesh er blitt gitt.

En litteraturstudie med hovedfokus på komponenter i fortøynings systemer og ankerlinebrudd ble presentert. Utviklingen til linebrudd de siste 20 årene har blitt illustrert gjennom statistiske data.

FAGLÆRER:	Professor Jochen Köhler
VEILEDERE:	Professor Jochen Köhler, Professor Per Jahn Haagensen
UTFØRT VED:	Institutt for konstruksjonsteknikk, NTNU

MASTER'S THESIS 2016

for

Alexander Hoel

3D Scanning of Corroded Mooring Chain

1. Introduction

As the largest operator on the Norwegian continental shelf with licences in several oil and gas fields, Statoil ASA is one of the world's largest suppliers of oil and gas. Since the start-up in 1972, the company has been involved in the development of numerous fields, and many of the mooring systems on their structures are approaching the end of their design service lives. The primary function of mooring lines is to maintain floating structures within prescribed boundaries and thus secure both the lives of the personnel on board, the material goods and the environment. Failure of one or multiple lines is associated with severe consequences both in terms of costs and risk of casualties. Several research projects regarding mooring lines are initiated. Better understanding of the correlation between surface conditions and remaining operating life is one of several objectives.

2. Objective

The objective in this thesis work is to investigate 3D representations of corroded chain link surfaces.

3. Assignment description

The main topics in the thesis work will be as follows;

1. Literature review: Perform a literature review on relevant subjects regarding mooring lines and 3D scanning, which together with the two additional master's theses can make a good foundation for understanding the challenges involved in the project.
2. Feasibility study: Investigate the possibilities at NTNU for 3D scanning of corroded chain link surfaces.
3. 3D representation: If possible, 3D models representing chain surfaces are desired.
4. Area of application: Investigate usage of the representations in analyses regarding the remaining life of mooring lines.

The candidate may agree with the supervisors to pay particular attention to specific parts of the investigation, or to include other aspects than those already mentioned.

PREFACE

This master thesis is written on behalf of the Department of Structural Engineering at the Norwegian University of Science and Technology. It concludes a master's degree in Mechanical Engineering and is the final result of work carried out during the spring semester of 2016 in Trondheim.

The assignment emerged through a collaboration between the university and Statoil ASA, from now on referred to as Statoil. As of today, the company has initiated several research projects regarding the mooring lines on their off shore structures. Better understanding of the correlation between surface conditions and remaining operating life is one of several objectives.

A collaborative project work on the same topic was carried out during the autumn semester of 2015 by the author, Martin Hove and Kristin Hanem Tømmervåg, resulting in the report *Assessment of the life of offshore mooring chains* (Hoel et al., 2015). The three individual theses from the mentioned authors may be considered as continuation of the project work.

The target group for this thesis is readers with prior knowledge of mechanical behaviour of materials, fatigue analysis and software based on the finite element method. The thesis deals with offshore mooring lines and 3D representation technology, but prior knowledge of these subjects is not necessary.

In working with this thesis, I have gained a lot of knowledge of the subjects fatigue, 3D representation and numerical modelling. Its has been a challenging and educational work. I have been fortunate enough to work with real life challenges in the industry and been given free hands when working with high quality and expensive technical equipment. I am grateful for the gained knowledge and my own personal development throughout the semester.

Alexander Hoel

Trondheim 15.July.2016

ACKNOWLEDGEMENTS

I would like to extend my gratitude's to my supervisors Per Jahn Haagensen and Jochen Köhler for their guidance with both the project work and with my thesis. To always be able to drop by your office for a discussion of either the thesis or more casual subjects, have been most appreciated.

Further gratitude's must be expressed to my colleagues Martin Hove, Kristin Hanem Tømmervåg, Truls Braut Bache and Tobias Rønneberg for our cooperation through the last year at the university. Working with you has lifted my spirit as well as the quality of my thesis. Such an open task would doubtlessly have been less rewarding without our discussions in late nights at the office.

Big thanks are given to Odd Kristian Nerdahl and Kristian Frugone for showing such interest in my project. Never have I been let down when asking for help in the laboratory at the Department of Structural Engineering. Also the people I met during my feasibility study, in Theoharis Theoharis, Øystein Skotheim, Knut Ragnar Holm, Torbjørn Hallgren and Knut Sørby, deserves my gratitude.

Special thanks is given to Sigmund Kyrre Ås for guiding me in my work in numerous occasions, even though you had no obligations for doing such. Your advices regarding the numerical analysis has been utmost appreciated.

And finally I would like to thank my father for invaluable feedback on the report and, most importantly, for your unshakable faith in me.

A.H.

ABSTRACT

This thesis is concerned with mooring line failure and 3D representations of corroded chain surfaces. Equipment for making such representations have been evaluated through a feasibility study carried out at NTNU.

An *ATOS III* sensor was used to measure heavily corroded chain surfaces. Measuring procedures have been evaluated and best practice has been suggested. The produced output was a dense point cloud, mapping an area of approximately 15 500 mm².

The point cloud was post processed in *Geomagic Studio 14* and *ANSYS ICEM CFD*. A surface model processed for inspection routines, was created. Also a model representing a block with a single cavity was made. This was compatible with the software Abaqus.

A submodeling analysis was carried out in Abaqus, to simulate a cavity on the surface of a chain link in static tension. Good conformity was found in the stress response of the edge regions. It was concluded that the submodel was able to recreate the conditions in a chain link surface. Consistency in the location of the critical area of the model was observed. Convergence of the maximum principle stress in the critical area was not proven. The smoothing routine and insufficient minimum size of the elements in the mesh was pointed out as the most plausible explanations.

The use of submodeling analysis in further study is highlighted as a good method for evaluating worst case scenarios considering cavities on the surface of chain links. Advices considering efficiently evaluation of convergence and mesh requirements have been given.

A literature study with main focus on mooring system components and mooring line failure was presented. The historical development considering mooring line failure during the last 20 years was illustrated through statistical data.

CONTENTS

Preface	i
Acknowledgements	iii
Abstract	v
Contents	vii
Acronyms	ix
1 Introduction	1
1.1 Motivation	1
1.2 Joint project	2
1.3 Objectives	2
1.4 Scope and limitations	3
1.5 Overview of thesis	3
2 Mooring Lines	5
2.1 Operations Offshore	5
2.2 System configuration	6
2.3 Mooring chain links	10
3 Essential Theory	15
3.1 Materials science	15
3.1.1 Material behaviour	15
3.1.2 Corrosion	15
3.2 Materials mechanics	17
3.3 The finite element method	19
3.4 Fatigue	20
3.5 Characterization of Surface Topography	20
3.6 3D Scanning Technology	21
4 Mooring failure	23
4.1 Regulations and procedures	23
4.2 Severity of mooring line failure	26
4.3 Historical incidents	27
4.4 Failure statistics	28
4.5 Fatigue testing of retrieved chain lengths	32
5 Feasibility Study	35
5.1 Artec Eva	35
5.2 Shapecrafter 3D	36
5.3 Agisoft PhotoScan and PhotoModeler Scanner	37
5.4 Konica Minolta	38
5.5 LEICA T-Scan AT901	38
5.6 ATOS III SO	39
6 Experimental Study	41
6.1 Equipment	41
6.2 Preliminary study	43
6.3 Preliminary results	44
6.4 Experimental setup and procedure	44
6.5 Experimental results	46

6.6 Discussion	48
7 Modelling	49
7.1 The surface model	49
7.2 The cavity model	52
8 Submodeling in Abaqus	57
8.1 Sub modelling	57
8.2 The global model	58
8.3 The submodel	59
8.4 Results	61
8.4.1 The global model	61
8.4.2 The submodel	62
8.5 Discussion	64
8.6 Possibilities and limitations	67
9 Concluding remarks	69
10 Future work	73
Bibliography	80
A 3D representation at NTNU	81
B Shapcrafter 3D	83
C Agisoft Photoscan	85
D Konica Minolta	87
E The surface model	89
F The cavity model	91
G Equipment for verification purposes	93

ACRONYMS

ASTM	ASTM International.
AT61	ATOS v6.1.
BAT	Department of Civil and Transport Engineering.
C3D10	10-node tetrahedron with quadratic interpolated displacement field.
C3D20	20-node hexahedron with quadratic interpolated displacement field.
C3D4	4-node tetrahedron with linear interpolated displacement field.
CLS	Chain Link Specimen.
CTO	Chief Technology Officer.
DFU	Defined hazard and accident situations.
FEA	Finite Element Analysis.
FEM	Finite Element Method.
FPSO	Floating production, storage and offloading unit.
FPSs	Floating Production Systems.
FSUs	Floating storage units.
GOM	Gesellschaft für Optische Messtechnik mbH.
GS14	Geomagic Studio 2014.
HMI	Hexagon Manufacturing Intelligence.
IACS	International Association of Classification Societies.
ICEM	ANSYS ICEM CFD 17.0.
IDI	Department of Computer and Information Science.
IPK	Department of Production and Quality Engineering.
IPM	Department of Engineering Design and Materials.
ISM	Initial Surface Model.
JIP	Joint Industry Project.
KT	Department of Structural Engineering.
NCS	Norwegian Continental Shelf.
NPD	Norwegian Petroleum Directorate.
NTNU	Norwegian University of Science and Technology.
PSA	Petroleum Safety Authority in Norway.
RNNP	Trends in risk level on the Norwegian Continental Shelf.
SPM	Single Point Mooring.
TLPs	Tension Leg Platforms.

TO Test object.

INTRODUCTION

1.1 Motivation

Mooring lines are vital components off shore. In the oil and gas industry, the primary function of mooring lines is to maintain floating structures within prescribed boundaries and thus secure both the lives of the personnel on board, the material goods and the environment. Failure of one or multiple lines is associated with severe consequences both in terms of costs and risk of casualties. Systems today are typically designed to withstand loads equivalent to a 100 year storm and with service lives of 20 years or more. This leads to substantial quality requirements, especially for systems in the North Sea where the environment is particularly harsh.

As the largest operator on the Norwegian continental shelf with licences in several oil and gas fields, *Statoil ASA* is one of the world's largest suppliers of oil and gas (*Statoil worldwide: Norway*, 2013). Since the start-up in 1972, the company has been involved in the development of numerous fields, and many of the mooring systems on their structures are approaching the end of their design service lives.

Chain links of high quality steel is widely used in off shore mooring systems due to their favourable mechanical properties. In the unfriendly environment, mooring lines are constantly subjected to degradation mechanisms such as wear and corrosion in addition to fatigue, which reduce the integrity of the systems. When inspecting chain links that have been in active service, the surface is often found to be altered due to the mentioned degradation mechanisms during their long service lives. As of today the correlation between surface conditions on chain links and their remaining lives is not fully understood, and the decision whether or not to replace a mooring line includes a substantial amount of uncertainty. As a safety measure, the mooring lines are replaced more frequent than assumed necessary. Better understanding of how the surface conditions affect service lives of the chain links could potentially reduce both costs and increase safety off shore. This is in the interest of Statoil as well as the oil and gas industry in general.

1.2 Joint project

The master's thesis work presented in this report is part of a collaborative project involving Statoil ASA and the Department of Structural Engineering at the Norwegian University of Science and Technology (NTNU). The final objective is to provide Statoil with tools for assessing surface conditions on mooring chain links in order to evaluate the remaining service life of the entire mooring line. Chain lengths, which have been in service on floating offshore structures for approximately 15 years, have been retrieved by Statoil to be studied at NTNU. Full scale fatigue testing is currently in process, where lengths of three chain links are subjected to cyclic tensile loading in a corrosive environment. The corrosion fatigue testing will provide the remaining lives of the lengths tested. At the time of writing, three master students, including the author, are involved in the joint project. Different topics are covered by the resulting theses. In order to obtain best possible understanding of the field of research and the progression of the joint project, the reader is referred to the theses of Martin Hove and Kristin Hanem Tømmervåg, to be published within summer of 2016, as well as a previous master thesis by Bjørnsen (2014). The reader should also be aware that a doctorate study and further master thesis studies are currently under development at the Department of Structural Engineering at NTNU.

Hoel, A., Tømmervåg, K.H. and Hove, M.

June 2016

1.3 Objectives

As explained in section 1.2, the main objective of the joint project, from now on referred to as *this- or the project*, is to better evaluate the remaining lives of mooring lines, based on the surface conditions of the chains. The focus in this thesis will be on 3D models representing the surface on corroded mooring chains, with the three following objectives:

1. Conducting a feasibility study of 3D scanning at NTNU.
2. Developing 3D representations of corroded chain surfaces.
3. Investigating possible usage of the representations in analyses regarding the remaining life of mooring lines.

1.4 Scope and limitations

The scope of the thesis is confined to:

- A limited feasibility study of available equipment for 3D representation at NTNU. Suitable equipment may have been overlooked and for this reason omitted in the report.
- The produced 3D representations are confined to limited areas of chain surfaces, and does not include complete chain link geometries.
- Due to the master's thesis work being part of a collaborative project, the subjects corrosion and crack growth are only briefly discussed in this report.

1.5 Overview of thesis

An overview of the content in each chapter are presented below.

Chapter 2 – Mooring lines: Common offshore systems and components are presented, with main focus on mooring chain links.

Chapter 3 – Essential theory: The chapter is concerned with the theoretical background for the content in this thesis.

Chapter 4 - Mooring failure: Regulations, procedures, possible consequences and statistical data regarding mooring line failure, are presented. Also a description of corrosion fatigue testing of retrieved chain lengths can be found here.

Chapter 5 – Feasibility Study: The chapter presents the results of the feasibility study. It describes the evaluated equipment and discuss possible usage in the project.

Chapter 6 – Experimental Study: The experimental setup for producing 3D representations of chain surfaces is presented. Discussion around the results follows.

Chapter 7 – Modelling: The chapter is concerned with post processing of the experimental results. Two models are presented: A surface model representing an area of a chain link surface, and a volume model representing a single cavity on the same surface.

Chapter 8 - Submodelling in Abaqus: In this chapter, a submodel analysis on the volume model from the preceding chapter, is presented.

Chapter 9 – Concluding remarks: In this chapter the results from the thesis work are summarised and assessed.

Chapter 10 – Future Work: Suggestions for further work are presented.

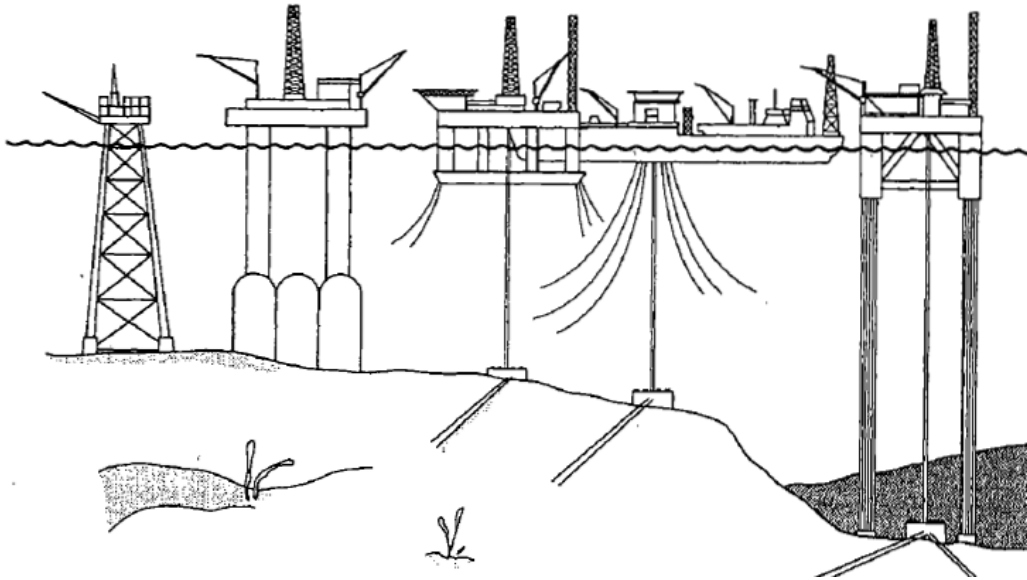


Figure 2.1: Illustration of five different offshore structures (Faltinsen, 1990, p. 2).

To fully understand the challenges involved with life assessment of mooring lines, some basic knowledge about floating offshore structures and associated components is required. This chapter is devoted to give a brief presentation of some systems and components offshore. More in depth attention is given steel chain links due to their relevance in this thesis.

2.1 Operations Offshore

The choice of structure type and system configuration for operations offshore depends both on the nature of the operations and the environment at site. In figure 2.1 five different offshore structures are illustrated. The two first structures from left to right, a jacket and a gravity platform respectively, are fixed structures that penetrate the sea bed. The following three structures are floating and represent a semi-submersible, a floating production unit and a tension leg platform respectively. While the tension leg platform is restrained against vertical movement using tethers (vertical tensioned anchor lines), the semi-submersible and the floating production unit are free floating and kept in position by different mooring sys-

tems (Faltinsen, 1990, p. 1). To secure personnel onboard and prevent material damages, structures need to be held in place in all kinds of weather. This is especially challenging in the hostile environment of the North Sea, where many of Statoil's sites are located. A typical mooring system design criterion is to be able to withstand a storm with a return period of 100 years. This criterion must also be met towards the end of the design service life, which is typically around 20 years (Noble Denton Europe Limited, 2006, p. 65). When taking the degradation mechanisms during service life into account, the extent of the challenge becomes apparent.

2.2 System configuration

A floating body has six degrees of freedom, resulting in six rigid body motions as illustrated in Figure 2.2. When describing motions at sea, the translatory motions are referred to as heave, surge and sway. Surge and sway describes motions in the horizontal plane and heave describes vertical motion. The three angular motions are referred to as roll, pitch and yaw. Yaw describes rotation around the vertical axis while roll and pitch describes rotation around the longitudinal and the latitudinal axis respectively (Faltinsen, 1990, p. 3). A mooring system counteracts these motions and keeps a structure on its location within given tol-

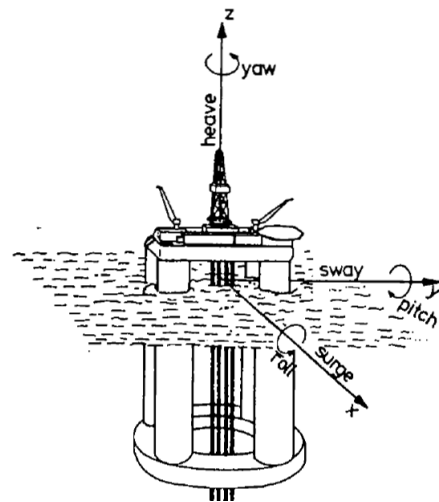


Figure 2.2: Rigid-body motion modes (Faltinsen, 1990, p. 3).

erances. According to Noble Denton Europe Limited (2006, p.22), “the primary purpose of a mooring system is to maintain a floating structure on station within a specified tolerance, typically based on an offset limit determined from the configuration of the risers”. Risers are pipes which transport hydrocarbons, injection fluids and other liquids between the subsea structures and the floating unit. The risers may play the part as limiting factor due to the need of reducing their vertical motion.

When designing mooring systems, Spread Moored- and [Single Point Mooring \(SPM\)](#) systems are the two most common configurations. In a spread mooring system the lines are connected to the structure in multiple areas. The structure will then be fixed in a certain orien-

tation and will not weather-vane. When a vessel is weather-vaneing it changes orientation with the direction of the environmental loading. Spread mooring systems is often cheaper than SPMs due to reduced complexity. They are typically used on semi-submersible units and non-weather-vaneing FPSOs (Floating production, storage and offloading units) in areas with moderate environmental loadings. In areas with rougher environments, such as the North Sea, spread mooring systems are less suitable due to the resulting forces exerted on the structure and its mooring lines. SPMs allow the floating structure to weather-vane and hence reduce the resulting forces. The mooring lines are then connected to the structure in a single point, with the aid of turrets as illustrated with an arrow in figure 2.4. A Turret is a connection point for risers and mooring lines and can be both externally connected and internally integrated in the floating structure. While the external turret systems are cheaper and less complicated than internal systems, the latter are preferred in the most hostile environments and when a substantial amount of risers and mooring lines should be connected to the turret. In some cases, such as in areas with typhoons or considerable risks of drifting icebergs, the turret system can be disconnectable (Mack et al., 1995, p. 14). Figure 2.9 illustrates the internal, disconnectable turret system on the Terra Nova FPSO.

Another important choice of design, is the principle of generating resisting forces. Catenary systems and Taut Leg systems can both be used for SPM and spread moored systems. In a “taut-leg” system, the elasticity of the lines are producing the resisting forces. The anchors at the end of each line must resist both horizontal and vertical forces. In a “catenary” system the mooring lines are not stretched to the same extent and use the dead weight of the lines to produce the resisting forces. A substantial length of the lines rest horizontally on the bottom, anchored to the sea bed. Resisting forces are generated by lifting and lowering the lines (Noble Denton Europe Limited, 2006, p. 27). This results in only horizontal loads on the anchors. Buoyancy elements and weights can be attached to the lines to optimize the system. In deep water depths the taut-leg system is most commonly preferred in order to limit the offset of the floating structures and because the taut leg configuration occupy less area on the sea bed. To reduced weight and increased flexibiity, the lines then usually consist of ropes, rather than chains (Bjørnsen, 2014, p.41).

In order to optimise mechanical properties, the mooring lines often consist of several segments with different components and materials. Different combinations of steel chain, steel



Figure 2.3: *Spread Mooring.* Adapted by author from (Noble Denton Europe Limited, 2006, p. 26).



Figure 2.4: *Single Point Mooring.* Adapted by author from (Noble Denton Europe Limited, 2006, p. 22).

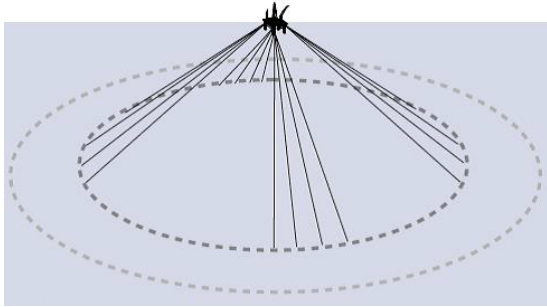


Figure 2.5: *Taut leg system* (Noble Denton Europe Limited, 2006, p. 29).

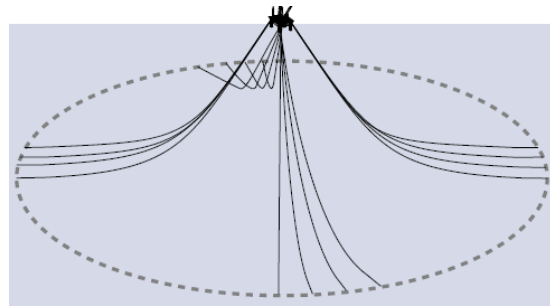


Figure 2.6: *Catenary system* (Noble Denton Europe Limited, 2006, p. 28).



Figure 2.7: *Anchor shackle.* Adapted by author from (Ramnäs Bruk, 2016).



Figure 2.8: *Chain emerging from trumpet* (Noble Denton Europe Limited, 2006, p. 132).

wire, natural- and synthetic fibre are common. Compared to lines composed of steel links exclusively, lines that replace some lengths with wire or fibre ropes are lighter and more flexible. In such segmented lines, steel chain links are often used in the beginning and end of the line providing necessary robustness in the most exposed areas.

The so called “Splashzone” is defined as five meters above the still water level and four meters below the still water level (Noble Denton Europe Limited, 2006, p. 102). Here, the lines are more subjected to certain corrosion mechanisms than in other segments. They may also be subjected to multiaxial loading. The part of the lines that contacts the seabed are exposed to particularly harsh conditions, in terms of degradation mechanisms and contact forces. Lifting and lowering of the lines, causes the chain links to slam down onto the seabed. This area is referred to as the “touch down area” or the “thrash zone” (Noble Denton Europe Limited, 2006, Appx. C p. 4). The dimensions of the links used in different segments of the line may also vary, depending on the desired weight and the expected wear in the specific area.

Shackles, connectors, fairleads and so called "trumpets" are other important components in a mooring line system. Shackles and connectors comes in many design variations and are used as connection points to the lines, for instance between the chain and the anchors. Fairleads and trumpets are mounted on the floating structure and used to guide and control the mooring line. Wear due to contact friction and out of plane bending, are some of the challenges associated with these components. Figure 2.7, 2.8 and 2.10 illustrates an anchor shackle, a submerged trumpet and a fairlead design respectively.

Anchors are the end point of the mooring lines and provide the resistance forces needed for station keeping of the floating structure. The design of the anchors depends on the size and direction of the loading through the mooring lines. Drag embedment anchors may withstand large horizontal loading by digging into the seabed, but cannot resist large vertical loads. They are thus not suitable for taut- leg mooring systems. Vertical load anchors, suction anchors and piled anchors on the other hand can withstand loading in any direction and may therefore be used for such systems. These are embedded in the seabed and their holding capacity depends on the lateral soil resistance of the seabed (Noble Denton Europe Limited, 2006, p.52).

In addition to mooring lines, a structure may be equipped with thrusters to adjust its position and in some cases reduce the acceleration in the event of a sudden movement due to rough

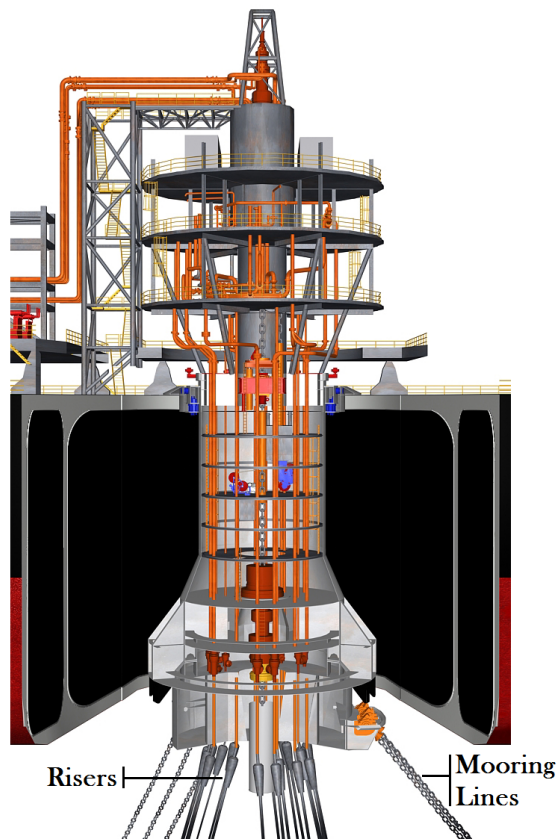


Figure 2.9: The Terra Nova Turret System. Adapted by author from (Howell et al., 2001, p. 10).

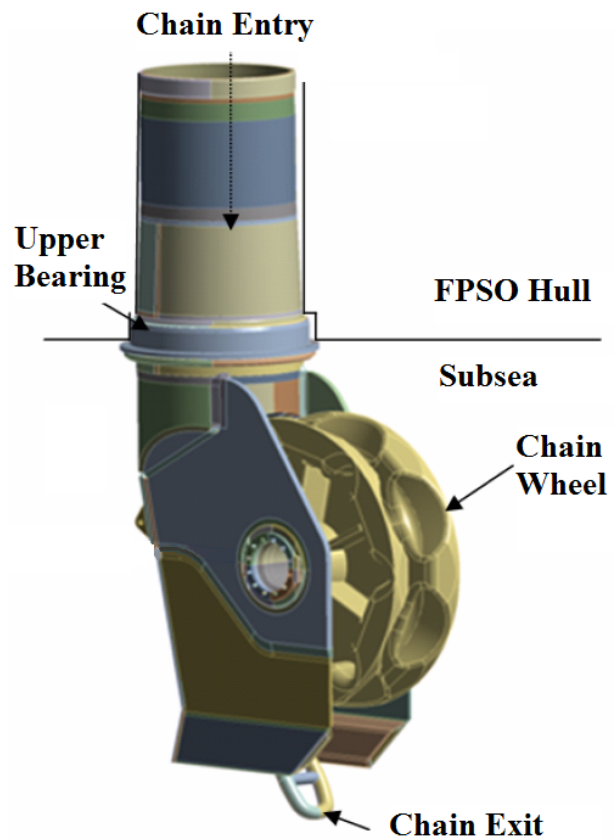
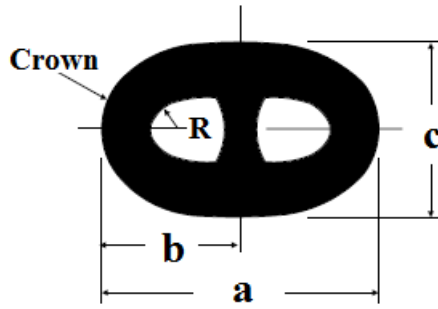


Figure 2.10: Example of a Fairlead design. Adapted by author from (McKeown et al., 2011, p. 3).

sea. Such thruster assistance can secure optimal tension in the lines, disperse wear more uniformly on the line and be a crucial safety measure in the event of failure. Another method to relieve the lines is by winching. The line is then pulled in or out to optimise the line load and to disperse wear to several chain links rather than one.

2.3 Mooring chain links

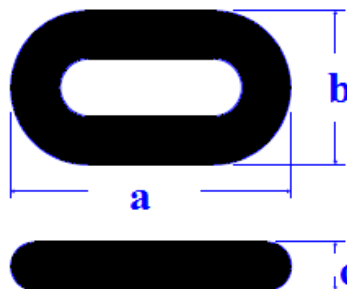
We often differ between two designs of chain links: Studded and Studdless. As the names implies, the studded link has a transverse stud across its inside width, while the studdless have none. When dimensioning chain links, the cross sectional diameter is determinative. All dimensions are scaled with the prevailing diameter as shown in figure 2.11. The two areas where the steel bar is bent are referred to as the crown of the chain link, as illustrated in figure 2.11a. Both DNV GL and the [International Association of Classification Societies \(IACS\)](#) provides guidelines for offshore mooring chains (DNV GL, 2015), (IACS, 2011, W22).



Designation (1)	Description	Nominal Dimension of the Link	Minus Tolerance	Plus Tolerance
a	Link Length	6d	0.15d	0.15d
b	Link Half Length	a*/2	0.1d	0.1d
c	Link Width	3.6d	0.09d	0.09d
e	Stud Angular Misalignment	0 degrees	4 degrees	4 degrees
R	Inner Radius	0.65d	0	----

Notes: 1 Dimension designation is shown in above figure
 d = Nominal diameter of chain, a* = Actual link length

(a) Dimensions and tolerances stud common link. Adapted by author from (IACS, 2011, W22, p. 14).



Designation (1)	Description	Nominal Dimension of the Link	Minus Tolerance	Plus Tolerance
a	Link Length	6d	0.15d	0.15d
b	Link Width	3.35d	0.09d	0.09d
R	Inner Radius	0.60d	0	----

Notes: 1 Dimension designation is shown in above figure.
 d = Nominal diameter of chain
 2 Other dimension ratios are subject to special approval.

(b) Dimensions and tolerances studless common link. Adapted by author from (IACS, 2011, W22, p. 14).

Figure 2.11: Dimensions and tolerances for studded and studless common link.

Although the production of the links follows standards, the exact dimensions of each link are difficult to establish due to some degree of plastic deformation during the production. Each link is therefore not equal in terms of dimensions, which introduce a challenge when inspecting wear on used chain links. Tolerances are provided to avoid to large deviations.

There are pros and cons related to both designs. For instance, the studded chain has greater stiffness and is less likely to knot or twist compared to the studdless, while the latter is lighter and easier to handle when it comes to accessibility (Noble Denton Europe Limited, 2006, p. 41). Both are used in the offshore industry today. Since the chain links examined and tested at NTNU are studdless, the focus in this thesis will be on this design.

As of today, the two main producers supplying Statoil with steel chain links, are the Spanish company Vicinay Cadenas S.A. and the Swedish company Ramnäs Bruk. The production procedure used by Ramnäs, starts initially with rolled steel bars which are heated with electrical resistance heaters, before being shaped into the geometry of links. The two ends of each steel bar are then flash butt welded together, a process where the bar is heated by the aid of electrical current before the ends are pressed together (Almar-Næss, 2009). Then follows trimming of the weld burr and heat treatment, where the links are tempered and quenched to obtain desired material properties like toughness and hardness. Using shotblasting, the surfaces is cleaned by multiple small particles which are blown towards the surfaces of the chain. To ensure that the chain links meet the prevailing high requirements, they are subjected to comprehensive testing and quality controls. Throughout the production process, dimensions and surface conditions of the links are inspected. Test specimens are collected for tensile-, break- and impact tests (Charpy V-notch). The links goes through proof loading tests, where about 70% of the minimum breaking load is applied. The interior of the welded areas are inspected with ultrasonic waves (Ramnäs Bruk, 2015, p.12).

Depending on their mechanical properties, steel chains are categorised with different grades. IACS (2011, p.174) denotes offshore mooring chains with the capital letter R followed by a number. Five different steel grades are used for mooring chains: R3, R3S, R4, R4S and R5. Their minimum mechanical properties are listed in figure 2.13.

The Charpy V-notch test is used to measure the toughness of a material. Sufficient toughness is required to avoid brittle fracture in the lowest temperature conditions expected in the design (Bjørnsen, 2014, p. 11). Brittle fracture can be defined as rapid fracture accompa-

Grade	Yield stress ⁴⁾	Tensile strength ⁴⁾	Elongation	Reduction of area	Charpy V-notch				
	R_e	R_m	A_5	Z	Temperature ¹⁾	Base		Weld	
	N/mm ²	N/mm ²	%	%		Average energy	Single energy	Average energy	Single energy
					°C	J	J	J	J
R3	410	690	17	50 ²⁾	0	60	45	50	38
					-20	40	30	30	23
R3S	490	770	15	50 ²⁾	0	65	49	53	40
					-20	45	34	33	25
R4	580	860	12	50 ³⁾	-20	50	38	36	27
R4S	700	960	12	50 ³⁾	-20	56	42	40	30
R5	760	1000	12	50 ³⁾	-20	58	44	42	32

1) For grade R3 and R3S, testing may be carried out at either 0°C or -20°C.

2) For cast accessories, the minimum value shall be 40%.

3) For cast accessories, the minimum value shall be 35%.

4) For guidance only: Typical yield to tensile strength ratio is in the range of 0.85 to 0.95. Tensile strength is normally not to exceed the minimum tensile strength with more than 150 MPa.

Figure 2.13: Minimum mechanical properties of mooring chain steel. Adapted by author from (DNV GL, 2015, p. 27).

nied by little plastic deformation (Dowling, 2013, p. 5). The test consists of using a swinging pendulum to break a notched test piece of certain geometry. By calculating the difference in potential energy, the absorbed energy is determined. The temperature conditions during test execution, are of significant relevance. Different temperature conditions causes different impact values to the materials (Norsk Standard, 2011, p.2).

When selecting steel grades, steels with too high yield stress is often considered undesirable. There is a common understanding that high strength steels with yield stress above 1300 MPa are more prone to hydrogen assisted cracking (Kvitrud and Bache, 2014, p. 8). Steel grade R4 is the standard grade on Statoil platform and higher grades are less commonly used.

This chapter provide general theoretical background for the content in this thesis. The reader is presumed to have prior knowledge in the fields: material science, material mechanics, fatigue analysis and the finite element method. The sections presented are intended to refresh the knowledge of the reader. For thorough introduction to the fields corrosion and crack growth analysis regarding mooring chain links, the reader is referred to the thesis work of Tømmervåg (2016) and Hove (2016).

3.1 Materials science

3.1.1 Material behaviour

If a material has the same properties in every location within the solid, it is defined as a *homogeneous* material. Materials where the properties are the same in all directions, are said to be *Isotropic*. For some metals, these idealised definitions are approximately true when considering the material at macroscopic size scales (Dowling, 2013, p. 202).

3.1.2 Corrosion

Corrosion is an electrochemical process, which can be described as surface wastage occurring when metals are exposed to reactive environments. For corrosion to take place, the formation of a *corrosion cell* composed of a cathode, an anode, an electrolyte and a metallic

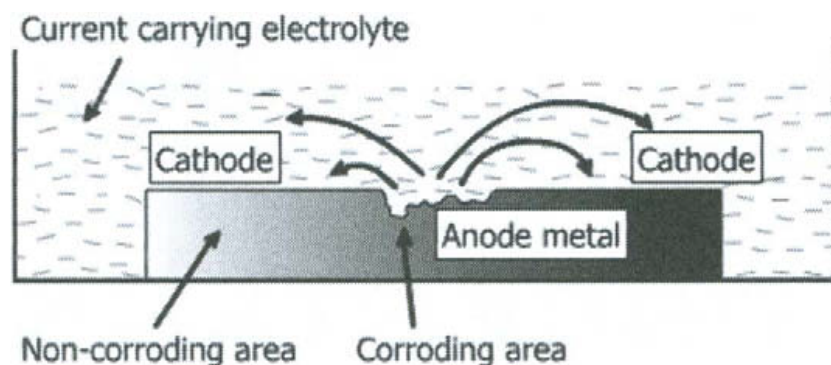


Figure 3.1: A corrosion cell (Ahmad, 2006, p. 10).

path, is required. Figure 3.1 illustrates the principle. An electrolyte is an electrically conductive solution, e.g. sea water. The corroding metal usually play the part as the metallic path.

Oxidation reactions takes place at the anode and cause loss of material when metal ions travels from the metal and enters the electrolyte. Equation 3.1 describes this reaction.



The metal ions might also react with the solution and form as precipitation on the surface. Equation 3.2 explains the dissolution of ferrous hydroxide at the anode location. This is commonly known as rust formation.



At the cathode, electrons released from the anode reactions are consumed. This is called a reduction reaction. Equation 3.3 explain the cathodic reaction where Hydrogen gas are produced in an acid solution (Ahmad, 2006, p. 9-12).



Pitting corrosion can be defined as localized corrosion on a metal surface. Cavities or pits forms when corrosion happens preferentially in small areas, leaving most of the surface untouched. The growth are unpredictable an may form as squares, circles and pyramids (Ahmad, 2006, p. 149).

The [ASTM International \(ASTM\)](#) provides a guide for examination and evaluation of corrosion pitting in (ASTM International, 2005). When describing the shape of pits by the shape of the cross sections, the terms shown in figure 3.2 are used.

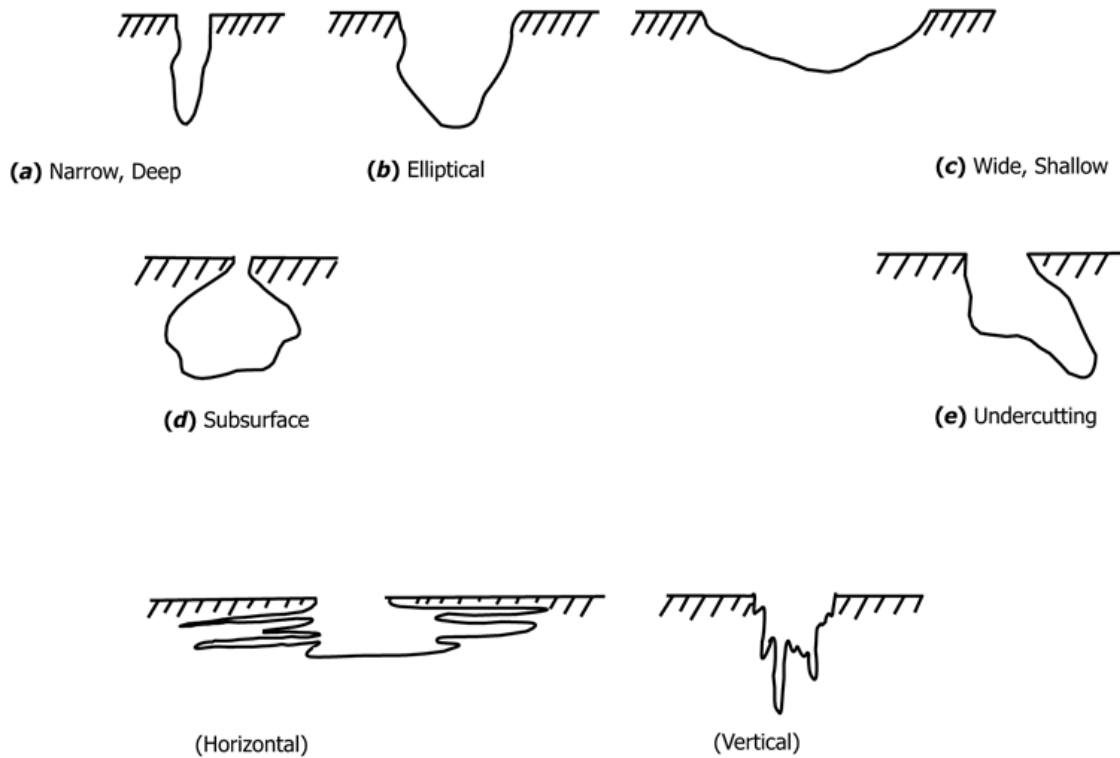


Figure 3.2: Description of pit geometry by cross sectional shape (ASTM International, 2005, p. 2).

3.2 Materials mechanics

When exposing a deformable object to a load, it will deform. Strain is a measure of relative deformation and is in one dimensional form defined as

$$\varepsilon_i = \frac{\Delta L}{L_i} \quad (3.4)$$

where L_i refer to the initial length of the object, while ΔL refer to the change in the length (Dowling, 2013, p. 203).

In any arbitrary point, the stress state can be completely described with the normal stresses in three directions, σ_x , σ_y and σ_z , and the shear stress on three planes τ_{xy} , τ_{yz} and τ_{zx} , as illustrated in figure 3.3.

If deformations are reversible, and the relationship between stresses and strains are linear, the material is defined as *linear elastic*.

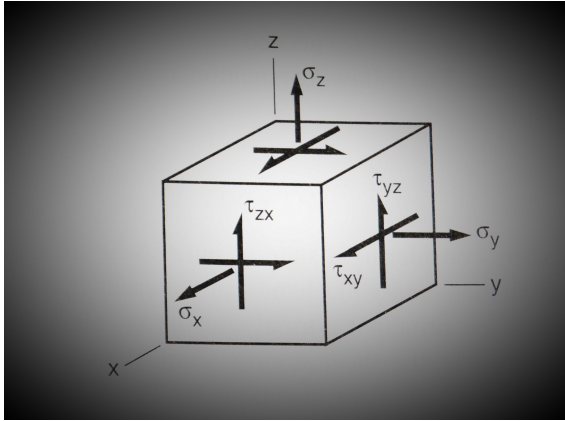


Figure 3.3: State of stress in an arbitrary point. Adapted by author from (Dowling, 2013, p. 205).

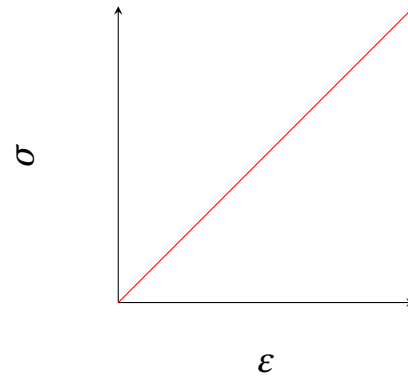


Figure 3.4: Linear elastic material behaviour

When assuming linear elastic material and small-strain theory, the relation between stress and strain may be described with the *generalized Hooke's law* through equations 3.5-3.10.

$$\varepsilon_x = \frac{1}{E} [\sigma_x - \nu(\sigma_y + \sigma_z)] \quad (3.5)$$

$$\varepsilon_y = \frac{1}{E} [\sigma_y - \nu(\sigma_x + \sigma_z)] \quad (3.6)$$

$$\varepsilon_z = \frac{1}{E} [\sigma_z - \nu(\sigma_x + \sigma_y)] \quad (3.7)$$

$$\gamma_{xy} = \frac{\tau_{xy}}{G} \quad (3.8)$$

$$\gamma_{yz} = \frac{\tau_{yz}}{G} \quad (3.9)$$

$$\gamma_{zx} = \frac{\tau_{zx}}{G} \quad (3.10)$$

E is the Young's modulus, ν the the elastic Poisson's ratio and G is the shear modulus. For a one dimensional stress state, Hook's law reduces to

$$\sigma = E\epsilon \quad (3.11)$$

The *principal normal stresses* are defined as the maximum and minimum values of the normal stresses, given in equation 3.2. On planes where the principal normal stresses occur, the shear stress is found to be zero (Dowling, 2013, p. 237).

$$\sigma_1, \sigma_2 = \frac{\sigma_x + \sigma_y}{2} \pm \sqrt{\left(\frac{\sigma_x - \sigma_y}{2}\right)^2 + \tau_{xy}^2} \quad (3.12)$$

3.3 The finite element method

The [Finite Element Method \(FEM\)](#) is a numerical method for solving boundary value problems. In [Finite Element Analysis \(FEA\)](#), a physical problem is idealised into a mathematical model. In order to solve this mathematical problem, the model is discretized by dividing it into a mesh with elements of finite size. Each element has a certain amount of nodes and degrees of freedom. By solving sets of linear algebraic equations for every element, nodal values, e.g. displacements are obtained. Field values, such as stress and strains, are found for the whole model by interpolating nodal values (Cook et al., 2002, p. 1-4) and (Mathisen, 2015, p. 5).

As [FEM](#) is a numerical solution, errors may be presented through the idealization and discretization of the model. Also the numerical solution for the discretized model may introduce errors. To state with sufficient certainty that a calculated solution is close to the real value, convergence should be demonstrated. A converging solution should decline steadily as the mesh is refined for each succeeding analysis, before approaching a certain value. Figure 3.7 demonstrates the principle.

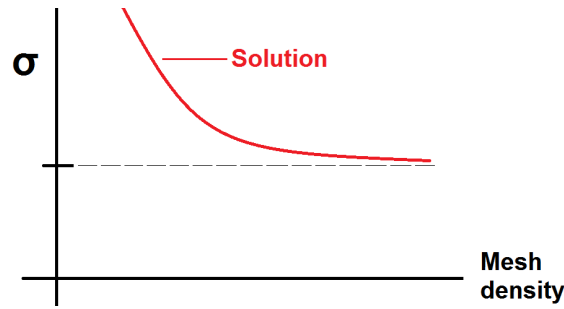


Figure 3.5: A hypothetically converging solution.

3.4 Fatigue

In a process where a component is subjected to cyclic loading, microscopic damages may occur in the material. This may occur even if the resulting stresses in the material are low. The microscopic damage is accumulated until a crack develops, which leads to failure of the component. Such a process due to cyclic loading is commonly referred to as *fatigue* (Dowling, 2013, p. 417).

The *fatigue life* of a component is defined as the number of cycles a component may endure during cyclic loading, before failure (ASTM International, 2013, p. 8). It may be decomposed into life before and life after crack initiation as follows

$$N_t = N_i + N_p$$

3.5 Characterization of Surface Topography

When characterising surface topography, statistical surface parameters are the most widely used (Stachowiak and Batchelor, 2006, p. 466). *The roughness average, R_a , and the root mean square roughness, R_q ,* are parameters describing the height characteristics of a surface and are given in equation 3.5 and 3.5.

$$R_a = \frac{1}{L} \int_0^L |z^2| dx \quad (3.13)$$

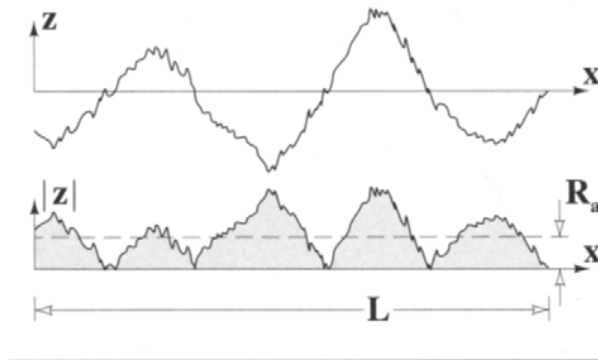


Figure 3.6: Finding the roughness average (Stachowiak and Batchelor, 2006, p. 467).

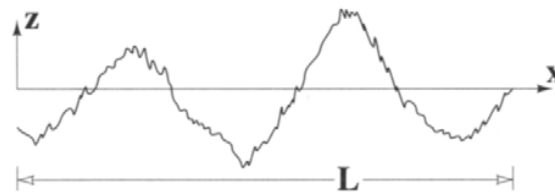


Figure 3.7: Finding the root mean square (Stachowiak and Batchelor, 2006, p. 467).

$$R_q = \sqrt{\frac{1}{L} \int_0^L |z^2| dx} \quad (3.14)$$

3.6 3D Scanning Technology

A 3D scanner is a device which analyse an object in order to obtain data of its shape and possibly its colours. They can be divided by their measuring principles, where division between contact- and non-contact scanner are common. Contact scanners, such as coordinate measuring machines, are not relevant for this project and will therefore not be further discussed (Moe, 2006, p.7).

Non-contact scanner may be further divided into *passive* and *active* scanners. While active scanners omit some kind of radiation, before detecting the reflected values, the passive scanners depend only on reflected ambient radiation.

Many non-contact measuring procedures rely on the *principle of triangulation*. Triangulation is described as the process of finding coordinates by using known triangle values. By using trigonometry and geometric theory, unknown lengths and angles can be found from known values (Moe, 2006, p. 12)

In the measuring technique of *Photogrammetry*, two dimensional photographs are converted into three dimensions. The technique is based on the triangulation principle, where photographs are taken from two or more locations. Rays from each camera to points on the object are developed and mathematically intersected to produce coordinates of three dimensions (Moe, 2006, p. 14).

Scanners using the *Structured-Light* principle are active scanners, often consisting of a sensor and one or more cameras. The scanner projects a light pattern on the object to be measured, and analyses the distorted image. From pixel values and calibration data, 3D coordinates are calculated (Moe, 2006, p. 24).

For further reading on the subjects presented, or on other principles, such as laser scanning and focus variation, the reader is referred to (Moe, 2006).

MOORING FAILURE

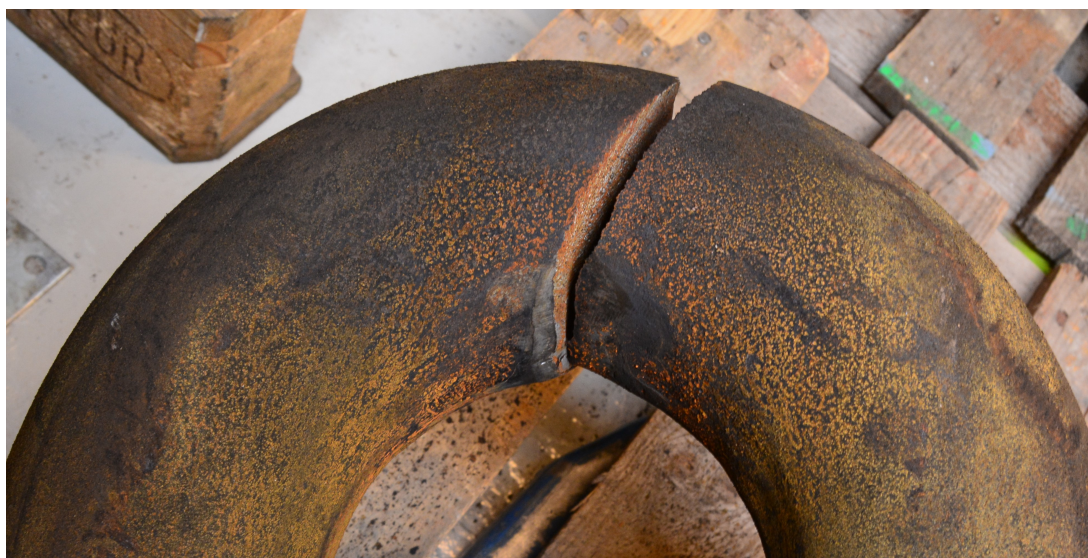


Figure 4.1: Failure of a corrosion fatigue tested chain link.

Where the Norwegian petroleum activity previously was dominated by developments, the trend today is dominated by operation of facilities (Petroleum Safety Authority Norway, 2016b, p.20). Many of the offshore structures are approaching the end of their design lives, and some mooring systems have more than 20 years in service. This chapter is concerned with mooring line failure. Regulations, procedures and consequences regarding failure is presented, in addition to statistical data. The corrosion fatigue testing carried out at [KT](#) at the time of writing is briefly presented in the last section.

4.1 Regulations and procedures

Regulations at the time of writing, states that flotels and production facilities should tolerate loss of two lines without serious consequences. The corresponding requirement for mobile drilling facilities is loss of one line without serious consequences (Petroleum Safety Authority Norway, 2016c, p. 28). The mooring systems should in other words be designed to tolerate at least a single line failure. However, the [Petroleum Safety Authority in Norway \(PSA\)](#) consider it as an undesirable incident (Petroleum Safety Authority Norway, 2016b, p. 125). The line

could cause severe damage to the subsea installation and may be a threat to the risers in the case of strong currents offsetting them. Operating with fewer lines than prescribed in the design criteria's will increase the loading on the remaining lines and thus increase the risk of additional failures.

In the event of a failure, the anchoring regulations still prevails. This means that the facility should tolerate additional failure after the initial one. The operator may have the opportunity to continue operation, if the environmental conditions allows for it. A common procedure is to analyse the event of line breakage, in order to find which weather conditions that require a shut down. If the production or drilling operations are shut down, the consequences of additional line breakage could be reduced, and in such cases lower safety factors than during state of operation is allowed (Norwegian Maritime Authority, 2009), (Petroleum Safety Authority Norway, 2016a, §3) and (Petroleum Safety Authority Norway, 2015, §63).

The procedures to replace the lost line may be both time consuming and costly. A [Joint Industry Project \(JIP\)](#) was carried out by Noble Denton between 2003 and 2004, aiming to improve the integrity of the mooring systems on [Floating Production Systems \(FPSs\)](#). In their report they illustrate a potential failure scenario, shown in table 4.1. Incidents with multiple line failures are not as frequent as with single line failures. However, they do occur, as presented in section 4.3 and 4.4. According to Noble Denton Europe Limited (2006, p. 79) the likelihood of multiple line failure increases in the case of systematic weakness in the mooring system design, if loss of a line goes undetected or if several lines in the same area suffer from degradation to the same extent. Table 4.2 illustrates a possible scenario following a multiple line failure.

The financial cost of mooring failure is high. Noble Denton Europe Limited (2006) investigated the so called *Business Interruption Impact* in the event of failure and replacement of one line. A hypothetical scenario involving a medium sized North Sea FPSO, with a capacity of producing 50000 (barrels per day) was first considered. When assuming two days stop in production, available spares and the mobilisation of two anchor handler tugs and a Dive Support Vessels, a cost of approximately 2 million GBP was estimated. In this estimate the costs of spare equipment was not included. Many sites lack spare parts and provision of new equipment may take months. Also a large West African FPSO, producing 250 000 bpd, where considered. With the same assumptions, the estimated cost was calculated to as much as

Table 4.1: *A potential single failure scenario (Noble Denton Europe Limited, 2006, p. 78).*

Deterioration ↓	The progressive deterioration of a component of the system under fatigue, corrosion or wear
Failure ↓	Followed by failure of the component under moderate storm conditions
Detection ↓	Line loss might be detected through tension monitoring equipment where that is installed. It is possible that the line failure could be undetected until a routine subsea check of the mooring system
Shutdown ↓	The system is likely to be shutdown until the continued integrity of the mooring system has been verified and new operating limits defined
Inspection ↓	The mooring and production systems would be inspected to identify any related damage
Reduced operations ↓	Resumption of operations under reduced weather criteria
Repair	Reinstatement of the full mooring system.

10.5 million GBP, due to bigger capacity and longer mobilisation time. The cost estimates presented involve a great amount of uncertainty and the extent of the costs are depending on the individual sites. However, the estimates clearly illustrates that mooring line failure is a great economical burden. Two main conclusions considering failures are drawn:

"Financial costs associated with mooring line failure are large, particularly relative to the capital cost of the failed component" (Noble Denton Europe Limited, 2006, p.84).

"Both lost production and vessel costs are significant" (Noble Denton Europe Limited, 2006, p.84).

Table 4.2: A potential multiple failure scenario (Noble Denton Europe Limited, 2006, p. 80)

Deterioration	The progressive deterioration of a type of component under fatigue, corrosion or wear
↓	
1st Failure	Followed by failure of the component under moderate storm conditions. This could go undetected
↓	
Unzipping	Overload of adjacent lines, perhaps after further deterioration if the initial failure was undetected
↓	
Excursion	Loss of integrity of the mooring system could be identified from the loss of station keeping after failure of several lines
↓	
Shutdown	The risers should be de-pressurized and isolated prior to damaging distortions in the system

4.2 Severity of mooring line failure

Vinnem (2001, p. 12) present findings from the research project “Operational Safety of FPSOs”. When taking personnel consequences exclusively into account, multiple failures in the mooring system are ranked as safety critical risk category one, which is the most severe category.

Also PSA evaluate the risk of mooring line failure, and describe itself as “an independent government regulator with responsibility for safety, emergency preparedness and the working environment in the Norwegian petroleum industry” (Petroleum Safety Authority Norway, 2016d). They have regulatory authority on the [Norwegian Continental Shelf \(NCS\)](#) in addition to several plants and pipelines systems. Emergency preparedness, working environment in the petroleum industry, and technical and operational safety are fields in which PSA serves as a regulator. When presenting and quantifying risk, PSA uses the definition *Defined hazard and accident situations* or so called [DFUs](#). The DFUs are meant to cover every possible scenario that may lead to loss of lives. The first twelve DFUs are associated with a “major accident risk”. The base definition PSA use when referring to a major accident is:

"A major accident is an accident (i.e. entails a loss) where at least three to five people may be exposed" (Petroleum Safety Authority Norway, 2016f, p.8).

"A major accident is an accident caused by failure of one or more of the system's built-in safety and emergency preparedness barriers" (Petroleum Safety Authority Norway, 2016f, p.8).

Loss of mooring system integrity is included in DFU 8, *Damage to platform structure/ stability/ anchoring/ positioning fault*. E.g. mooring line failure is associated with major accident risk.

4.3 Historical incidents

Mooring line failure may lead to severe consequences, like loss of station, which in turn may develop to a risk of collision with surrounding structures. The incident with *Eide Barge 33* as recently as December 2015, was not caused by a mooring line failure, but illustrates the severity of losing station. A failure of the tow at the towing boat *Eide Wrestler* caused the barge to freely drift in the south of the North Sea towards the installations at the field *Valhall* with a velocity of around 2 m/s. The 100 meter long barge passed Valhall by less than 2 km, causing 380 of the personnel at site to be evacuated (Petroleum Safety Authority Norway, 2016b, p. 121), (Norwegian Broadcasting Corporation, 2015).

Another possible consequence of losing station involves damage to the risers, with following risk of hydrocarbon spill. In 2004, two lines payed out and were lost on the semi-submersible *Ocean vanguard* due to failures in the brakes. The structure drifted 160 meters off position resulting in fracture of the riser, damage to the Blowout Preventer and loss of the well (Kvitrud and Bache, 2014, p. 5). Kvitrud and Vinnem (2006, p. 23) consider the event as serious and states that only luck prevented severe consequences.

The FPSO (Floating production, storage and offloading unit) *Petrojarl 1* lost two lines almost simultaneously in 1994 after being hit by a 20-25 meter high wave. Two additional line failures followed, resulting in four of eight lines with lost capacity. The FPSO was able to keep position due to thruster assistance, but the production was shut down. No personnel was evacuated (Noble Denton Europe Limited, 2006, p. 76).

In 1981 *North Sea Pioneer*, a converted drilling rig previously named *Argyll Transworld 58*,

suffered multiple line failures after only six years in service, with a complete loss of station as result. An initial failure was followed by four additional ones. To prevent from more uncontrolled failures and the risk of capsizing, the crew cut three of the remaining four lines. One line was kept intact to prevent the rig from crashing into surrounding structures. The rig drifted freely for a total of 1.5 days before being secured with towlines. 48 people were evacuated and the production was deferred (Noble Denton Europe Limited, 2006, p. 66). The severity of capsizing may be illustrated with the Alexander Kielland accident in 1980, causing 123 fatalities (Hagland, 2015).

4.4 Failure statistics

In the late 90s, the [Norwegian Petroleum Directorate \(NPD\)](#) aimed to develop a tool for monitoring the development in risk level on the NCS. During 1999-2000, the project [Trends in risk level on the Norwegian Continental Shelf \(RNNP\)](#) was initiated. The work of the project is continuous and presented annually, with the first report being published in 2001. RNNP has been carried out by PSA since 2004 (Petroleum Safety Authority Norway, 2016e).

In their report from 2006 on behalf of PSA, Kvitrud and Vinnem (2006, p. 2) conclude that the number of incidents involving mooring lines on the NCS are too high. Even with the assumption of under-reporting before 2000, an alarming amount of incidents between 1996 and 2005 had been reported. The frequency of events on the NCS corresponded to one failure for every ten facility years (Kvitrud and Bache, 2014, p. 18). Several reasons were pointed out and the most common failure modes were found to happen in the components which constitutes the actual line. Failure in shackles were found to be disturbingly frequent compared to the relatively modest amount of shackles on a line. Also fatigue failures of steel chain links due to bending were found to be a common failure mode, where poorly design of the fairlead systems were pointed out as a possible explanation. Increased knowledge among the crew offshore, better systems for knowledge sharing and more focus on maintenance were suggested (Kvitrud and Bache, 2014, p. 6). With the increased focus on failures in mooring system, the industry reacted and a decline in the development of incidents could be observed.

After several years with positive development, an increase of incidents after 2010 was observed. Both previously known and unknown failure modes occurred. Between 2010 and

2014 a total of 16 line failures were recorded. These were caused by fatigue, manufacturing errors, overloading and mechanical damage. Kvitrud and Bache (2014) investigate the line failures and compare them with data from the previous investigation from 2006. They conclude that once again a lift of the quality in the industry is needed and call for quality rising measures in the industry.

Table 4.3: Linefailures on the NCS between 2010 and 2015. Adapted by author from (Petroleum Safety Authority Norway, 2016b, p. 126).

Component	Fatigue	Overload	Mechanical damage	Manufacturing errors
Chains	3	3		2
Socket				1
Steel Wires		2 ^a	1	
Kenter Link	1			
Fibre ropes			3	

^aBoth double line failures

In table 4.3 the 16 line failures are illustrated, sorted on the components that failed and the cause of failure. Both of the two incidents of overloading of steel wire cables resulted in double line failures. In their report, Kvitrud and Bache (2014, p. 19) investigate eight incidents with two or more line failures between 2000 and 2012 on the NCS, as shown in figure 4.2. The failure causes included fatigue, dragging of anchors, lines being payed out, anchor loss, ductile overload of steel wire ropes and overload of steel wires due to bending over the fairlead. In the incident with Brideford Dolphin in 2000, three lines failed.

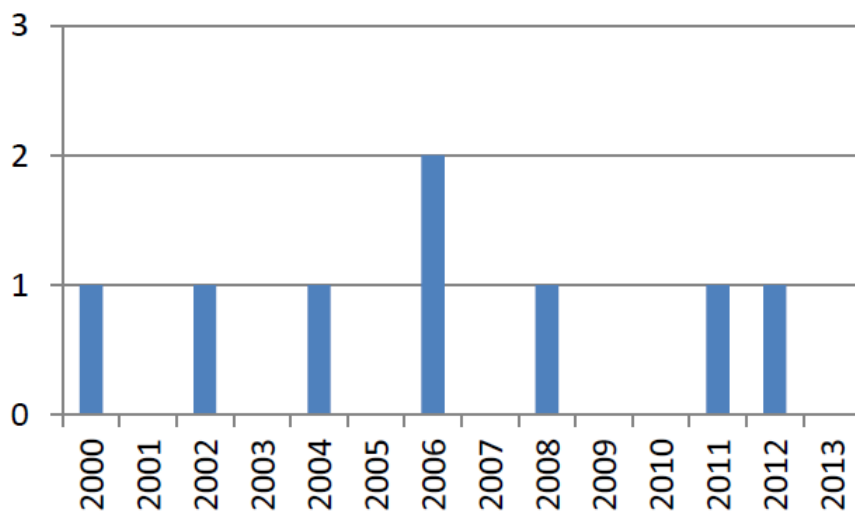


Figure 4.2: Incidents with two or three line failures on the NCS 2000-2012. Adapted by author from (Kvitrud and Bache, 2014, p. 19).

A failure rate of magnitude 9.2×10^{-3} per line year for single line failures were observed between 2010 and 2013. A rate of 1.2×10^{-3} was observed for double line failures in the same period (Kvitrud and Bache, 2014, p. 4). When comparing the failures that occurred on the NCS between 2010 and 2014 with data from the investigation in 2006, Kvitrud and Bache (2014, p. 18) conclude that the failure frequency has not improved over the past ten years. Possible changes in the quality of materials, maintenance, regulations and standards are proposed and discussed.

Not only data from the NCS, but also data from the British petroleum industry are included. Kvitrud and Bache (2014, p. 19) discuss Det Norske Veritas (2007)'s investigation of incidents in the UK between 1980 and 2001. Also this investigation presents notably high failure rates. Morandini and Legerstee (2009, p. 1) suggest, with reference to (Det Norske Veritas, 2007), a historical rate of mooring failures in the UK to be about:

- once every 1.5 operating years for drill ships,
- once every 4 operating years for drilling semisubmersibles,
- once every 7 operating years for FPSOs,
- once every 8 operating years for production semisubmersibles and
- once every 17 operating years for FSUs.

Kvitrud and Bache (2014, p. 19) do however point out the different practice in use of safety factors, when comparing data from the UK and the NCS.

In their most recent version of RNNP at the time of writing, Petroleum Safety Authority Norway (2016b, p. 125) presents statistics concerning mooring systems between 2000 and 2015. Figure 4.3 illustrates the number of recorded incidents where mooring lines have lost their load carrying capacity during operation. The incidents are defined in DFU8 and sorted after the number of failed lines. Blue columns illustrates incidents where one line has lost its load carrying capacity. Incidents where multiple lines have lost their load carrying capacity are represented with red columns. Figure 4.4 illustrates reported incidents that involve mooring lines and associated equipment. The incidents are sorted in the categories *Mobile units* and *Floating Production Units*. Mobile units includes semi-submersibles, jackups, drill ships and flotels used for drilling- and accommodation. The latter group includes semi submersibles, FPSOs and [Tension Leg Platforms \(TLPs\)](#) (Petroleum Safety Authority Norway, 2016b, p. 34).

Petroleum Safety Authority Norway (2016b, p. 2) concludes that much effort has been put in avoiding failure of mooring lines in recent years. No line failure has occurred between April 2014 and April 2016, the publish date of the report. Of the year 2015, only two incidents associated with mooring systems were reported, where none of these included line failure.

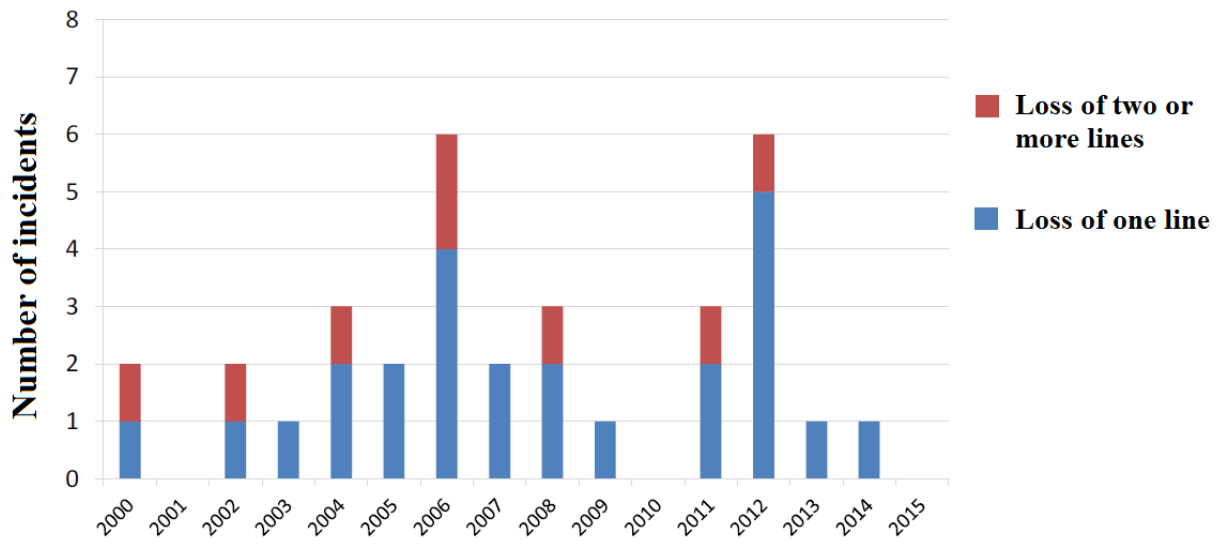


Figure 4.3: Incidents involving mooring lines with lost load carrying capacity. Adapted by author from (Petroleum Safety Authority Norway, 2016b, p. 127).

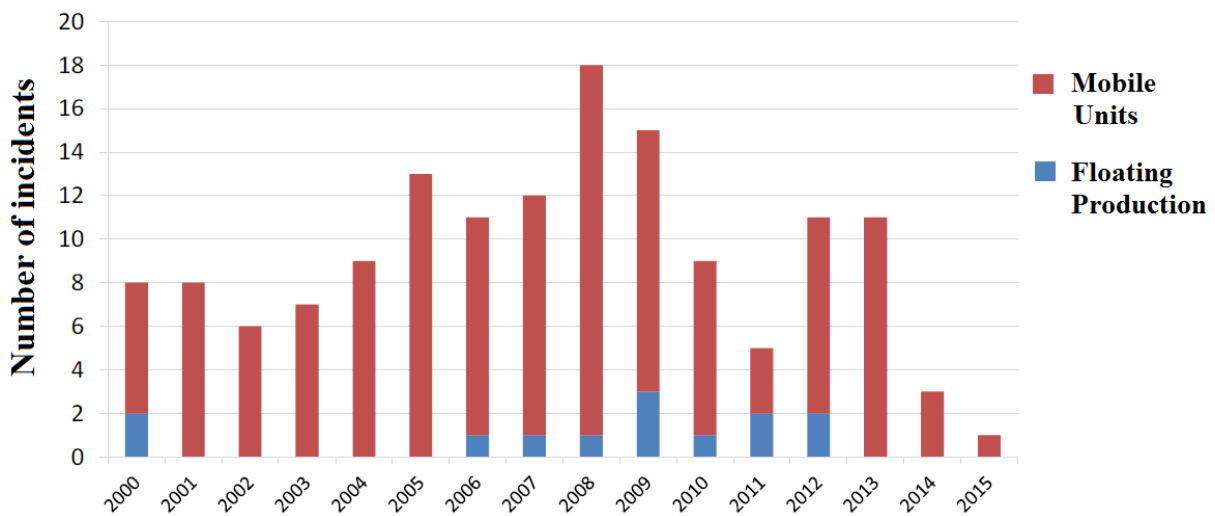


Figure 4.4: Reported incidents with mooring lines and associated equipment. Adapted by author from (Petroleum Safety Authority Norway, 2016b, p. 127).

4.5 Fatigue testing of retrieved chain lengths

As mentioned in section 1.2, corrosion fatigue testing of common studless mooring chain links with service lives of approximately 15 years was carried out at KT at the time of writing. Lengths of three chain links were mounted in a hydraulic testing machine and subjected to cyclic tensile loading in a corrosive environment until failure. Figure 4.5a shows the setup.

The condition of one of the retrieved links is shown in figure 4.5b. As can be seen, the surface was clearly altered by corrosion. The nature and extent of the corrosion on the lengths was varying. In some areas, the corrosion was evenly distributed, while in other areas, pits with depth of several millimetres could be found. A trend was observed, where the surface in the contact area between adjacent links tended to be smoothed down by interlink wear. As stated in section 1.3, an objective was to make 3D representations of chain surfaces. Due to the varying extent of corrosion, the utilised equipment had to be adaptable for several types of surface conditions.

The final results of the testing program would find the remaining lives of the retrieved lengths. Since the fatigue testing at KT was under progress at the time of writing, the results were not available for this thesis work. However, a trend was clearly present, where failure mostly occurred in the crown area, as shown in figure 4.5c. A similar fatigue testing program of retrieved common studless chain links was performed by Fredheim et al. (2013). Here, lengths of six links were subjected to axial tension corrosion fatigue testing. It was stated that all failure occurred in the bend- or crown region, where mostly initiation from the outside of the bend was observed.



(a) Fatigue testing machine. The grey chamber was filled with saltwater during testing.



(b) Surface condition of a retrieved link.



(c) Failure in the crown region of a tested chain link.

Figure 4.5: Corrosion fatigue testing of retrieved chain lengths

An important objective for this thesis work was to produce 3D representations of rough chain link surfaces. In order to achieve this, a thorough feasibility study was required. The participants in the project had little knowledge of the technology required and of the availability of suitable equipment at the university. In addition, it was desired that the author should carry out the measurements due to limited financial resources.

As a starting point, two requirements regarding the representations were decided. The equipment should be able to represent the surface with at least better accuracy than 1 mm and preferably better than 0.1 mm. In addition, the output files produced with the equipment had to be compatible with [Finite Element Analysis \(FEA\)](#)-based software. That is to say that, with or without post-processing of the results, it had to be possible to perform numerical analysis on the output files in software such as *Abaqus*. Finally, a portable device was preferable, but not a requirement. Each of the chain links to be scanned is heavy, with a mass of more than 100 kg. Arranging the tangled links before scanning is demanding and requires a lifting crane. A portable scanner would ease the procedure and probably save a fair amount of time.

This chapter presents the most relevant equipment assessed during the feasibility study, carried out between January and February 2016, along with the author's evaluation of its suitability for the project. Section [5.6](#) treats the equipment which was considered as best suited for the project and therefore used in further work. Table [A.1](#) in appendix [A](#) summarise the findings. Table [G.1](#) presents equipment with high accuracy which potentially could be used to verify measurement results.

5.1 Artec Eva

The [Department of Computer and Information Science \(IDI\)](#) at NTNU owns a handheld scanner and associated software from the producer *Artec 3D*. The producer offers several types of handheld scanners, where the IDI has acquired the *Artec Eva* model. The scanner is based on structured-light triangulation and the producer claims a 3D resolution of 0.5

mm and a 3D point accuracy of 0.1 mm. Colour information of 24 bits per pixel (bpp), 1.3 megapixel resolution, suitability for both reversed engineering and quality controls are other advantages highlighted by Artec 3D (Artec3D, 2016).

Due to the scanner's portability, claimed high resolution and good accuracy, Artec Eva was initially considered as a good option for the thesis work. However, after discussion with Prof., Theoharis at the IDI on February 24, 2016, the scanner was rejected. Previous work with the scanner, undertaken by personnel at IDI, had resulted in far worse accuracy than advertised. This may well have been caused by insufficient training, but due to limited time available for training in this project, no further investigation of the scanner was carried out. Another reason for rejecting the scanner, was the fact that no personnel experienced in the use of Artec Eva was available at IDI when the feasibility study was carried out.

5.2 Shapecrafter 3D

Shapecrafter 3D is a real-time 3D RGBD camera. With the aid of structured-light triangulation technology, 3D point clouds in full colour can be produced. The technology in the camera has been developed by SINTEF ICT since 2001 and the product was commercialised with the establishment of *ShapeCrafter AS* in July 2015. At the time of writing, the latest version of Shapecrafter 3D has a resolution of 2.3 Megapixels and can measure an area of 780×490 mm. With ideal conditions, the resolution range from 50 to $100 \mu\text{m}$. A prototype with a measuring area corresponding to an European pallet is currently under development. One of the main advantages with Shapecrafter 3D is the high acquisition rate. With a resolution of 2.3 Megapixels, Shapecrafter 3D may take snapshots with a rate of 12 Hz. This corresponds to a full 3D image in about 80 ms. With 1.2 Megapixels resolution, the acquisition rate could be doubled. The area of application is mainly industrial, where in-line inspection in manufacturing, 3D machine vision and 3D part localisation for robots are examples of possible usage (ShapeCrafter, 2016a), (ShapeCrafter, 2016b) and (ShapeCrafter, 2016c).

With the aid of co-founder and CTO at Shapecrafter AS, Øystein Skotheim, the camera was used for several measurements of chain link surfaces. Due to Skotheims expertise, the procedure was efficient and the output had high resolution. The result is illustrated in section B. Since Shapecrafter AS aims for industrial applications like part localisation, the associated software did not have any efficient procedure for merging, or so called "stitching", of

separate measurements at the time when the measurements were done (February 29, 2016). Merging was possible, but required a lot of manual work. Due to both the curved surfaces and the complex geometry of the cavities, several measurements with corresponding stitching was required to represent the chain surface. For this reason, although being the most efficient equipment tested in the feasibility study, Shapecrafter 3D was not considered the best option for this project.

5.3 Agisoft PhotoScan and PhotoModeler Scanner

3D modelling software based on photogrammetry can make textured 3D models from photographs taken with any digital camera. The quality of the model depends on the quality of the photos, which again depends on the resolution of the camera used and the photographers skills. *Agisoft PhotoScan* and *PhotoModeler Scanner* are such photogrammetric software available at NTNU. The [Department of Civil and Transport Engineering \(BAT\)](#) have licenses for Agisoft PhotoScan while IDI have licenses for the latter software. For close-range photography, Agisoft claims an absolute accuracy for their software of 1 mm (Agisoft, 2015, p. 2). PhotoModeler claims a relative accuracy of 1 in 8000 for high resolution photographs. This corresponds to an accuracy of 9×10^{-3} inches (≈ 0.23 mm) for a six foot object. When combining high resolution cameras with coded targets recognised by the software, the alleged accuracy is 1 part in 25000 (Eos Systems Inc, 2016), or in other words approximately 0.07 mm for a six foot object.

A test of 3D modelling with Agisoft PhotoScan was carried out by the author and Prof., Knut Ragnar Holm at BAT on February 19, 2016. Ten photos of a chain link piece were taken with a 16-megapixel *Samsung Galaxy S5 neo* mobile camera. No special adjustment of lighting conditions or any form of calibration were done. The photos were taken from different angles and used to create a 3D model in Agisoft PhotoScan. The result are presented in appendix C. The software was user friendly with a swift procedure. The accuracy, however, was difficult to state. Since the accuracy claimed by suppliers usually state the best possible outcome, it might differ substantial from the result obtained by inexperienced users. For this reason, the author consulted Prof., Torbjørn Hallgren at IDI on February 25, 2016. Based on his wide experience in photogrammetric software, Prof., Hallgren believed that the desired accuracy of 0.1 mm could be obtainable for this project using PhotoModeler Scanner, provided an experienced photographer and a high resolution camera with short focal length.

Since no personnel with experience with photography was available, the idea of using photogrammetric software in this project was rejected. However, capturing the geometry of chain links using photography, includes considerable mobility compared to the other methods assessed by the author. Provided the mentioned requirements being met, the author therefore consider photogrammetric software as a method with great potential when it comes to inspection of mooring chain links.

5.4 Konica Minolta

Konica Minolta Vivid 910 3D digitizer use laser triangulation to digitise 3D volumes. It is a so called “flying spot profiler” which emits stripes of light onto the object to be scanned (Schuman-Olsen et al., 2010, p. 36). By receiving and analysing the light reflected from the object, distance information of the object is recorded. It is used in terrestrial studies and in medical science among other fields and the producer reports accuracy of approximately 0.22 mm, provided specific conditions (Konica Minolta, 2006, p. 56 & 59). At the time of writing, BAT owns a version of the Vivid 910 model along with associated software.

Test scans were performed by the author and Prof., Knut Ragnar Holm at the BAT on February 19, 2016. The results are illustrated in appendix D. The digitizer produced point clouds with a density of about 50 000 measurement points per scan. Whether or not this density was sufficient, was questioned by the author, since the resulting polygon mesh clearly deviated from the actual surface of the chain. The associated software has functions for merging different measurements. This is highly relevant for the project, but the results of the merged test-scans revealed major defects, where the cavities on the surface tended to get filled up. Despite of the claimed accuracy of approximately 0.22 mm, Prof., Holm doubted better accuracy than 1 mm for the chain surface in this project, based on previous experience. For this reason, further trials with scans and merging were not performed.

5.5 LEICA T-Scan AT901

At the time of writing, [Hexagon Manufacturing Intelligence \(HMI\)](#) is lending the [Department of Production and Quality Engineering \(IPK\)](#) a *Leica Absolute Tracker AT901*. The measuring equipment is the preceding version of their latest model, the *AT960*. The Absolute Tracker is developed for measuring substantially larger measuring volumes than intended in this

project, but comes with an appurtenant handheld scanner intended for smaller volumes. The latest version of the handheld scanner, *Leica T-Scan 5*, claims accuracy of $\pm 60 \mu\text{m}$ and an acquisition rate of 210 000 measuring points per second. According to the producer, the handheld scanner does not require surface treatment of the object to be measured and may even measure shiny metallic and dark matte surfaces without photogrammetric targets (Hexagon Metrology, 2015).

On February 25, 2016, the author contacted Prof., Knut Sørby at the IPK, who is HMI's contact person regarding the lent measuring equipment. According to Prof., Sørby, a request for lending the handheld scanner could be presented HMI through the existing agreement. The likelihood of such an arrangement would increase in the case of involvement of multiple student projects and of potential customers (e.g. Statoil). If the handheld scanner could comply with the producer's promises, the Leica T-scan 5 could prove to be the best option when it comes scanning of chain surface, due to high accuracy combined with great mobility and no requirements for surface preparations. Due to limitations in time, the author chose not to go further with this possible arrangement. However, the author wants to highlight this possibility, if for instance large amount of chain links are to be scanned in future work. Further studies of costs involved with such an agreement and the scanners compatibility with rough chain surface is then advised.

5.6 ATOS III SO

The [Department of Structural Engineering \(KT\)](#) at NTNU holds an *ATOS III* sensor from the producer [Gesellschaft für Optische Messtechnik mbH \(GOM\)](#). The ATOS III system enables digitisation of object surfaces through a combination of structured-light and photogrammetry. During measurements, different fringe patterns are projected on the object to be measured while recording with two cameras. By using the triangulation principle, the system calculates the object's 3D coordinates. Measuring volumes within the range of $35 \times 28 \times 15 \text{ mm}^3$ up to $2000 \times 2000 \times 2000 \text{ mm}^3$ ($L \times W \times H$) is covered per scan, depending on the set of lenses being deployed. Large volumes may be digitised by merging (stitching) separate measurements and the results can be exported in several formats. Up to 4 million points per scan with accuracy of 0.03-0.08 mm is obtainable (Schuman-Olsen et al., 2010, p. 40) and (Gom mbH, 2008, p. 11).

ATOS III was purchased in 2006 when the laboratory *VIROPLAB* was established at the [Department of Engineering Design and Materials \(IPM\)](#). The laboratory was intended to introduce modern visualisation equipment into research and education at NTNU (Moe, 2006, p. 1). In 2012, the equipment was moved to the laboratory at the KT. During the feasibility study, it was discovered that neither personnel at the KT or at the IPM had any considerable knowledge about the equipment. The system had not been used regularly for years and personnel who had previously been involved with the system were either not longer present at NTNU, or had not maintained their previous knowledge. Strong interests for implementing the system in future work were present at KT. In order to evaluate the suitability of the system, the author consulted one of GOM mbHs distributors, *Cascade*, with offices in Sweden. According to Cascade, the ATOS III system was suitable for the intended work in the project and should be able to represent the degraded chain surface with accuracy better than 0.1 mm.

Being the only equipment that met the requirements, had functions for merging and was 100 % available with no additional cost for usage, the ATOS III system was considered as the best option for this project. However, the system suffered from years without regular usage and a lot of effort had to be put into debugging. Lack of experienced users constituted the biggest challenge. Of the more than 150 working hours spent in the laboratory, much time has been devoted into purely learning how to use the equipment. To update the KT on the gained knowledge, the author has demonstrated usage of ATOS III for personnel at the laboratory, and handed over relevant documents. Succeeding users are strongly advised to read [chapter 6](#) and the work of Bache (2016).

6.1 Equipment

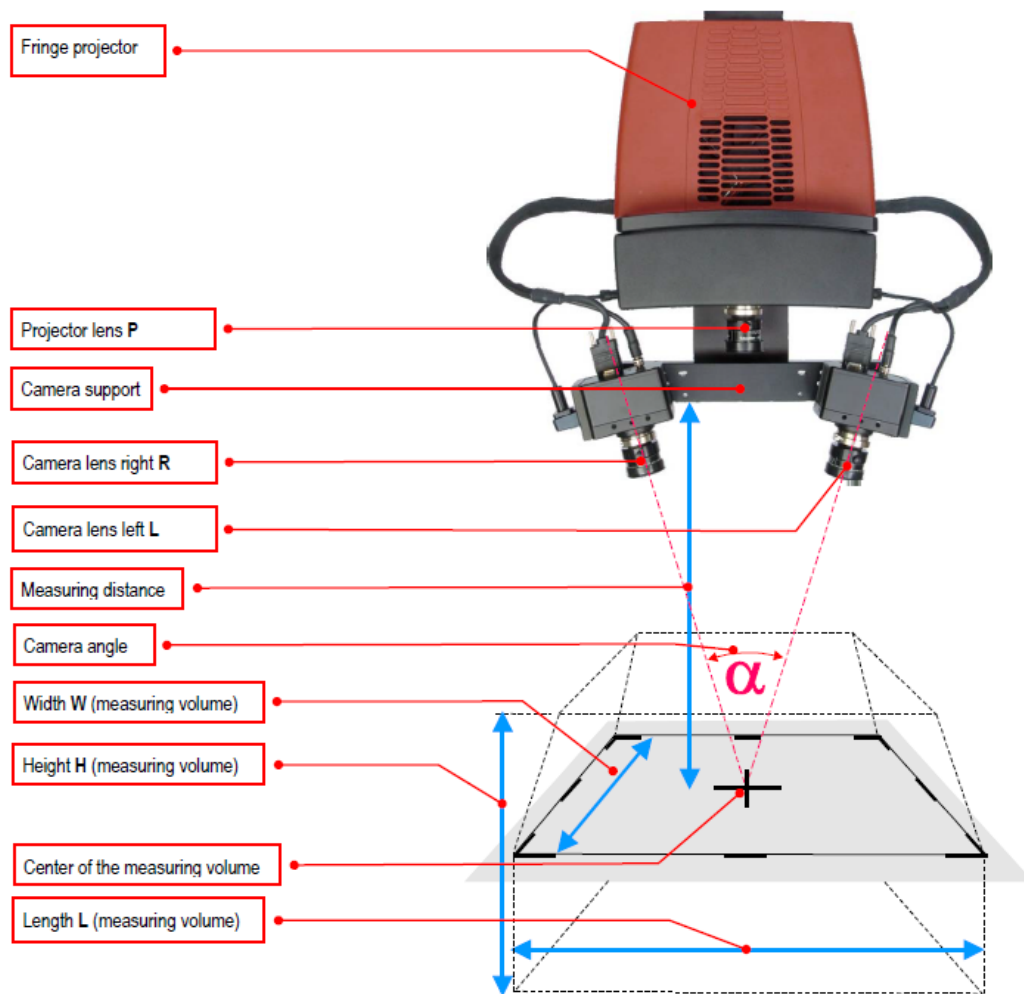


Figure 6.1: Configuration of ATOS III SO with component names and explanation of measuring parameters (Gom mbH, 2010, p. 9).

When measuring with ATOS III, the set of camera lenses and the projector to be used depends on the measuring volume. Figure 6.1 illustrates the sensor setup and explains some measuring parameters. The laboratory at KT is at present equipped with three sets of lenses with corresponding projectors: The SO MV 100-, the MV 550- and the MV1500 set. The number succeeding "MV" corresponds to the measuring volume of the set, where the number defines the sides of the quadratic area in the centre of the measuring volume, as illustrated in figure 6.1. After consultation with Cascade, the SO MV 100-set was used. This so called

Table 6.1: ATOS III SO specifications (Gom mbH, 2010, p. 7).

Min. measuring volume [mm ³]	Max. measuring volume [mm ³]	Measuring points per scan [-]	Camera resolution [pixels]
30 × 30 × 13	300 × 300 × 300	≈ 4 million	2048 × 2048

Table 6.2: Measuring Parameters (Gom mbH, 2010, p. 9).

Measuring volume (L × W × H) [mm ³]	Reference point size Ø [mm]	Measuring point distance [mm]	Focal length, projector lens [mm]	Focal length, camera lenses [mm]	Measuring distance [mm]	Calibration object [-]
100 × 100 × 80	0.8	0.05	23	50	450	CP30MV100x100

"SO configuration" is intended for smaller measuring volumes (SO = Small Objects) than the other two sets, and would achieve best possible representation of the deep cavities in the chain link surface. Table 6.1 shows system specifications, while table 6.2 shows the corresponding measuring parameters used, as instructed in the manuals.

When the results of multiple scans are to be merged, the use of reference points is required. These enables the software to align the different measurements. The measuring distance is the distance between the sensor and the object to be measured, as illustrated with a blue arrow in figure 6.1. Measuring point distance give information about the detail resolution, and gives the approximately distance between each measuring point on the surface of the measured object. With smaller measuring point distance follows better detail resolution (Gom mbH, 2008, p. 3, chap. C). To capture the cavities in the chain surface with best possible accuracy, a high number of measuring points per area is required, and thus the SO configuration was used. This ensured as small measuring point distance and hence the most points per area as possible. The measuring point distance is given by the resolution of the camera lenses and the measuring volume, which in this case is:

$$\frac{100 \text{ mm}}{2048} \approx 0.05 \text{ mm}$$

To be able to perform measurements, the system needs to be properly calibrated. The calibration process is intended to adjust the system optimally to the object which is to be measured. In this process, the sensor is used to take several snapshots of a calibration object from different angles and distances. The calibration objects have reference points with known exact dimensions, which the system use to adjust the system settings. The reference object



Figure 6.2: Calibration panel, CP30MV100x100.

used in this experiment, the *CP30MV100x100*, is shown in figure 6.2.

6.2 Preliminary study

The surface of the chain links suffer substantial degradation. On the worst locations, the surface has a complex geometry where the cavities may be several mm deep. In an attempt to optimise the measurement procedure, four test objects, from now on referred to as *TO1-4*, were initially scanned and the results were compared. The goal was to decide best practice concerning preparation of the object to be measured. Two objects were made by cutting out specimens of a chain link with particularly degraded surface. *TO1* was kept with its original surface, while *TO2* was sprayed white with a *Nord-test developer U89*, of the brand *Helling GmbH*. This is a so called "developer", used in crack inspection. The projected pattern on the surface of object to be measured needs sufficient contrast to be recorded by the cameras. The motivation for colouring *TO2* white, was to make the surface light and dull, and thus produce a pattern with enough contrast, according to the guidelines in the *ATOS manuals* (Gom mbH, 2008, p. 4, chap C). During the experimental work, it was proven difficult to capture the walls of the cavities, due to complex geometry. In an attempt to simplify this procedure, *TO3* and *TO4* were made as casts of the chain link surface on *TO1*. This was done by using the synthetic rubber replicating compound *101RF Fluid*, of the brand *Microset*. In this way, the cavities were represented inversely on the casts. *TO4* was sprayed white with the developer for the same reasons as with *TO2*. *TO1-4* are shown in figure 6.3.



Figure 6.3: The four test objects assessed, from left to right: TO1 with original chain surface, TO2 with coloured chain surface, TO3 as cast with original surface color and TO4 as cast with coloured surface.

6.3 Preliminary results

The white and the red border along the side of TO1 was made with marker pens, to identify the areas from where TO3 and TO4 originates. It was discovered that such borders were unfavourable. Especially the white border caused problems, as the sensor struggled with capturing the white (and highly reflective)- and the dark, corroded surface simultaneously. This was due to differences in brightness causing shutter time problems, which in turn resulted in lack of measuring points. An uniformly coloured surface was in other words to prefer. When examining TO3 and TO4, it was discovered that in some areas, the replication compound was not able to represent the cavities satisfactorily, due to air bubbles. In addition, when comparing the measuring results from TO1 with the ones from TO2, it was discovered that the results were not substantially improved when preparing the surface. In the case of inspection by scanning, as little additional work as possible is desired to keep the process time and costs down. For this reason TO2-4 was rejected, while TO1 was used in further work. Being the chosen specimen for further thesis work, TO1 was renamed to the [Chain Link Specimen](#) and is from now on referred to as the [CLS](#).

6.4 Experimental setup and procedure

Figure 6.4 and 6.5 illustrates the approximately geometry and the surface conditions of the CLS respectively. As can be seen in the picture, the surface suffer from substantial corrosion with deep cavities, resulting in a complex surface geometry. To allow merging of different measurements, reference points were attached to the surface. This can be seen as circular, black stickers, with white circles in the middle.



Figure 6.4: The CLS.



Figure 6.5: Surface conditions of the CLS.

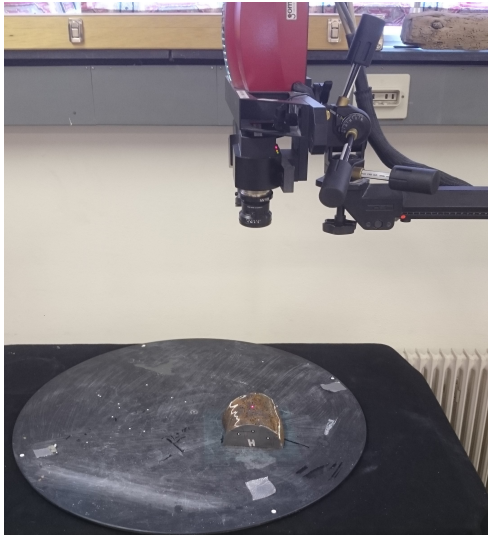


Figure 6.6: Measuring of the CLS, placed on a rotating table.

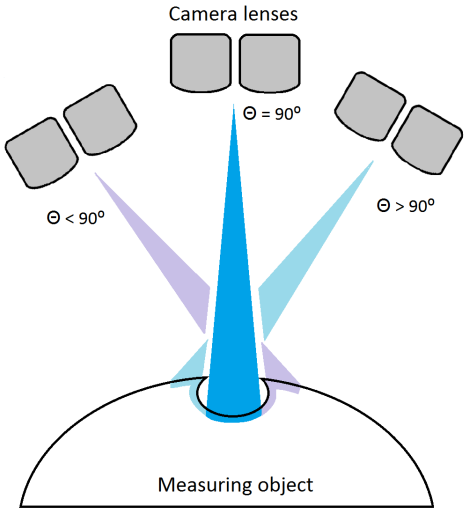


Figure 6.7: Illustration of measurement of a cavity from different angles.

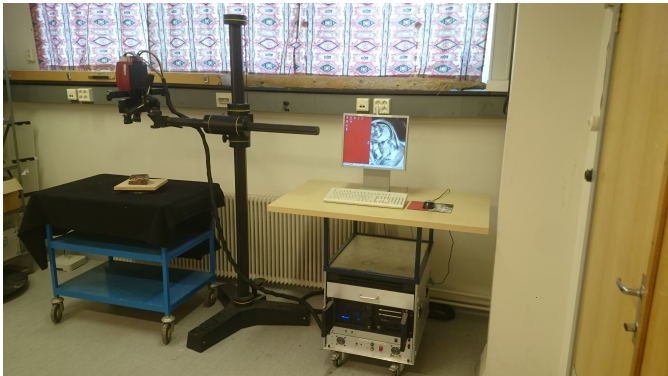


Figure 6.8: Experimental set-up showing the main system components and the CLS to be measured.

The main hardware components constituting the ATOS III system are the sensor head with projector and two cameras, a stand for holding the sensor head, power supply for the sensor and a PC system with Linux operating system. The software [ATOS v6.1](#), from now on referred to as [AT61](#), is installed on the PC and used to control the measuring procedure. During measurement, a live footage is shown in the software, and the user may update settings as shutter times, decide the area to be measured etc. The objects to be measured, were placed on a rotating table to ease scanning of different areas without changing the measurement distance. [Figure 6.8](#) shows the measuring setup.

Several scans were needed to cover the whole surface of the CLS. The geometry of the cavities were complex, and both subsurface and undercutting (as explained in [section 3.1.2](#)) was observed. For this reason, the scanner was not able to measure the walls of the cavities by only moving the objects in the horizontal plane. To provide sufficient angle to cover the walls, the CLS was tilted in various angles on the rotating table, while the camera lenses on the sensor were kept in the same position. [Figure 6.7](#) illustrates the principle of measuring the whole surface area of a cavity.

The surface on the CLS suffered from corrosion, which results in a non-uniform distribution of colours. For this reason, different areas of the surface reflected different amount of light. In order to measure the entire surface, different shutter times were required. In each measurement, a total of seven shutter times were used, ranging from 0.021 to 0.251 seconds.

A total of 12 measurements were carried out to cover a surface area on the CLS of approximately 15500 mm^2 . These measurements were aligned and "stitched" together in [AT61](#).

6.5 Experimental results

Due to the complex geometry, certain areas were not measured satisfactorily. Therefore, each measurement required evaluation and in some cases deselection of areas with errors. [Figure 6.9](#) is a snapshot from [AT61](#) and illustrates measuring errors. The software provides a triangulation mesh during measurements, based on the generated point cloud. The mesh is automatically updated when either new measurements are added, or old ones deleted. As can be seen in [figure 6.9](#), measuring areas of poor quality resulted in wrong representation of the surface, where cavities got "filled up" by triangles. To avoid this problem, low-quality areas were located on the existing measurements and their results deleted. [Figure 6.10](#) is an



Figure 6.9: Due to measuring errors, some cavities got "filled up" in the resulting triangle mesh.

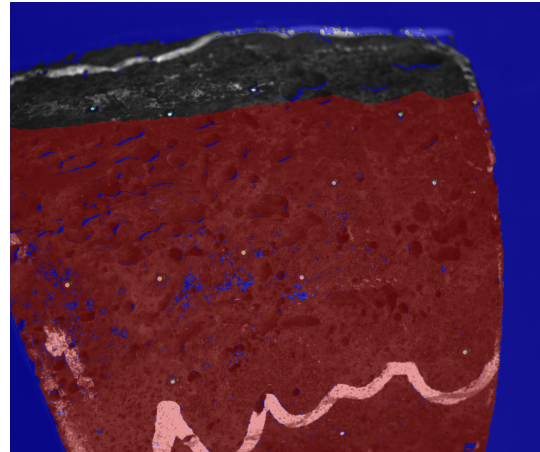


Figure 6.10: Deselecting measuring areas of bad quality.

other snapshot from AT61 and illustrates the results from one measurement. The software accept measuring points from red coloured areas, while results from dark areas are rejected. In the blue areas, no measurement points were registered by the system. As can be seen in the snapshot, blue areas appeared within the red area. On these locations the corrosion product was rubbed off, exposing shiny metal underneath. The amount of reflected light from the shiny spots was too high for the system to measure. Producing measuring points in such areas require additional post processing, and is discussed in section 7.1.

The debugging process resulted in a rough surface mesh model, consisting of 4 053 675 polygons. This **Initial Surface Model**, from now on referred to as the **ISM**, is illustrated in figure 6.11. The polygon mesh was automatically created by the software AT61, based on the measuring points produced. The green spots on the surface of the model represent reference points, used by the software in the stitching process. Eventough measurements were done with varying angles, some areas were not measured, resulting in holes in the surface mesh. Mesh errors like creased edges were also present. For this reason, the surface mesh model was exported for post-processing. Several formats are available for exporting from AT61, as described in table A.1. In this thesis work, the surface model was exported in .stl format for further post processing.

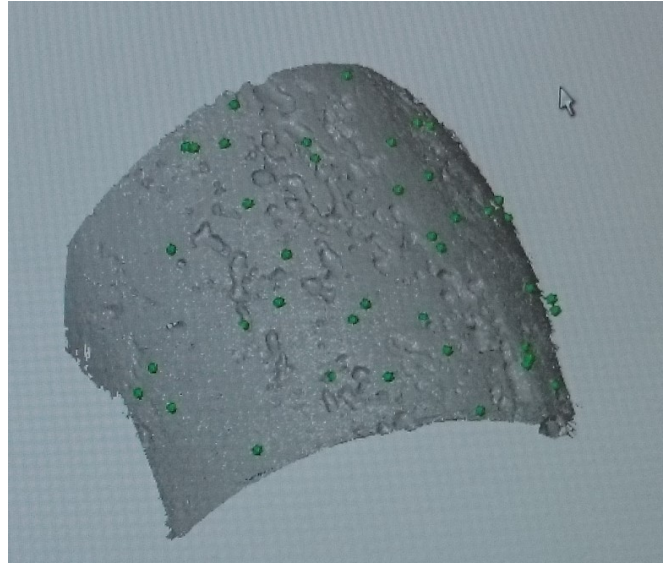


Figure 6.11: The initial surface model (ISM) of the CLS, created in AT61.

6.6 Discussion

The results from the experiment showed that the equipment was capable of capturing the complex surface geometry. For this reason, it was concluded that the selected equipment indeed could be used for further mapping of corroded chain link surfaces in the laboratory at [KT](#). However, it has to be pointed out that the procedure was rather time-consuming, and is at the time of writing not considered as a very effective inspection routine. The equipment was in addition sensitive for vibrations during measuring. For these reasons, the author doubt that the *ATOS III* sensor is a good option for inspection routines offshore.

To be able to perform analysis with the surface mesh created in AT61, some post processing is required. This chapter presents the process for creating two models. The first model is a surface model without thickness, representing the surface of the CLS. This is to be used in inspection routines, which will be further discussed in section 10. The second model presented is a 3D model consisting of volume elements, and will be used in a submodel analysis, presented in chapter 8.

7.1 The surface model

Post processing of measuring results is possible in AT61, which is installed on the computer in the laboratory at KT, directly connected to the ATOS III sensor. However, due to the age and state of the computer system which dates back to 2006, a more powerful computer was desired. Due to the size of the files to be handled, sufficient computer resources are essential. Licenses for the powerful software [Geomagic Studio 2014](#), from now on referred to as [GS14](#), are available for students at NTNU and enables processing of point clouds and surface meshes. For this reason, this software was used when post-processing the ISM created with AT61.

Figure 7.1 illustrates the imported ISM, presented with GS14. As can be seen, the model contained several errors. The green lines on the surface represents individual borders, and illustrates in this case flaws on the surface. An ideal representation should only have one continuous green border encircle the entire model. As explained in section 6.4, areas where the system was unable to produce measuring points resulted in holes in the mesh. Other mesh problems caused by the complex geometry were highly creased edges, self-intersections, spikes and small tunnels. The post-processing of the ISM in GS14 was done in multiple steps and will be described in the following. Table E.1 in appendix E provide more detailed information of the process.

The ISM consisted of a surface mesh with around 4.05 million polygons, which required a lot of repair work. To be able to do this, the model was converted to a point cloud model, which

required substantially less computer resources. The function *Convert to points* in GS14 allows for conversion of an existing polygon object to a point object by removing the polygons and maintaining the underlying points (Geomagic Support Center, 2016a). The resulting model consisted of around 2.15 million points. A clean-up process was carried out by removing points which would cause discontinuities in the polygon mesh. The function *Reduce noise* was used to remove measurement points caused by noise during the measuring procedure. In this process, the software use statistical methods to calculate the assumed locations for these points, before moving them there (Geomagic Support Center, 2016b). When the initial clean-up process was done, the amount of measuring points was reduced with 25 % by sampling with prioritisation of areas with high curvatures. GS14 enables retaining of points in highly curved areas like in the cavities, and reducing of the amount in flatter areas. The amount of points following the clean-up process was reduced to around 1.39 million points.

The point cloud model was converted back to a polygon mesh with the aid of the function *Wrap*. The software then produced a mesh of triangle elements, by using the measuring points in the point cloud. To limit the required computer resources for handling the model, the maximum amount of polygons was set to 1.7 million. A higher limit is possible and would result in a finer polygon mesh. The amount of errors in the new mesh was drastically reduced compared to the ISM. Still, some post-processing was required. The function *Meshdoctor* allows automatically localisation of mesh flaws, with succeeding repair work. This is one of the main strengths of GS14 and saves the user much time in the repairing process. The function was used for re-meshing areas with self-intersections, tunnels, spikes and highly creased edges. Due to the complexity of the holes in the mesh, *Meshdoctor* was not able to re-mesh holes to the authors satisfaction. For this reason, all holes were filled manually by the author. In the final part of the process, areas which was not meshed satisfactorily was manually deleted, before a final round with the *Meshdoctor* was carried out for smoothing purposes. The resulting surface mesh, from now on referred to as the surface model, consisted of triangle elements without flaws and covered an area of approximately 12300 mm². The size was reduced with almost 60 %, to around 1.64 million polygons, which substantially simplified further work with the model.

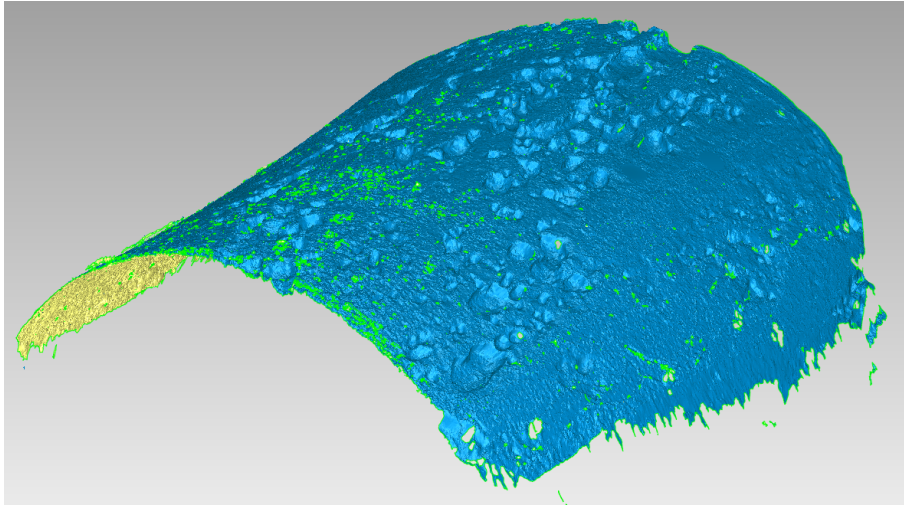


Figure 7.1: *The ISM imported in GS14.*

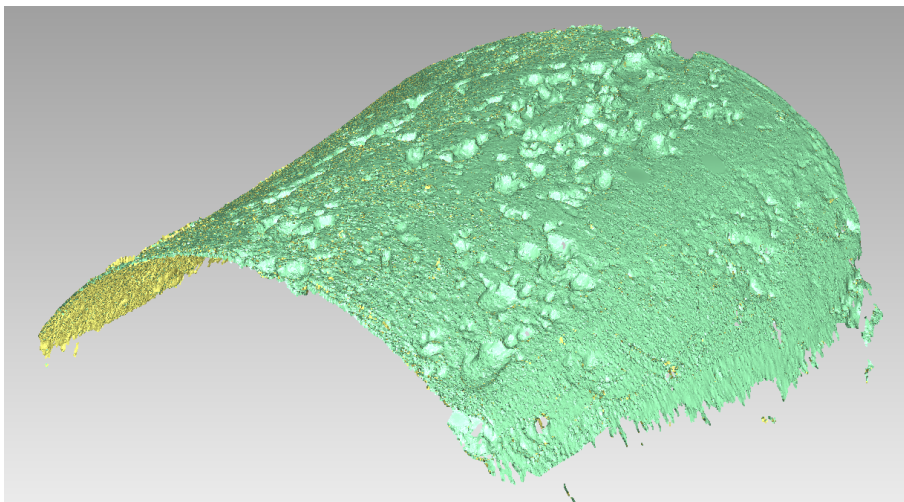


Figure 7.2: *ISM converted to a point cloud model.*

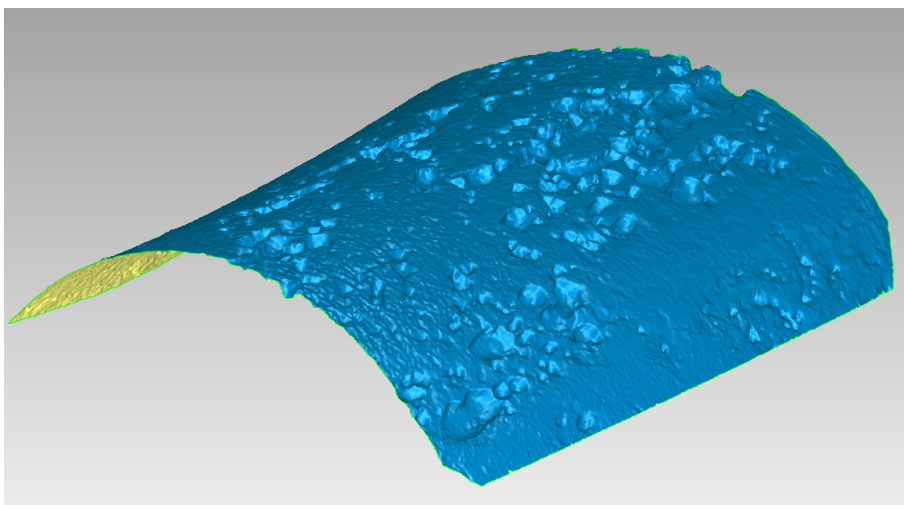


Figure 7.3: *The surface model resulting from post-processing of the ISM.*

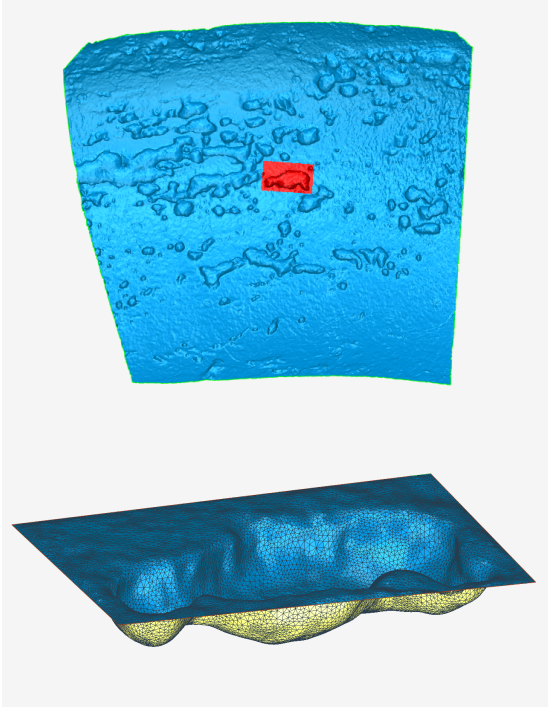
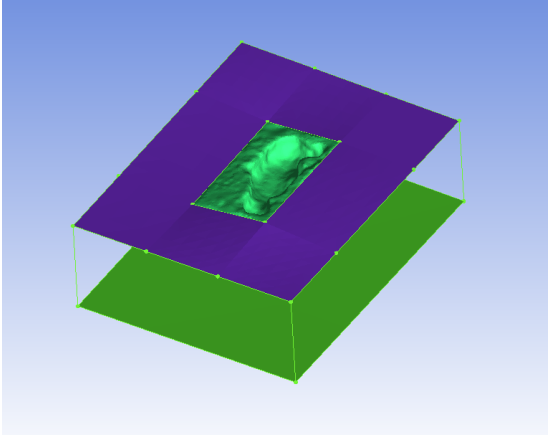
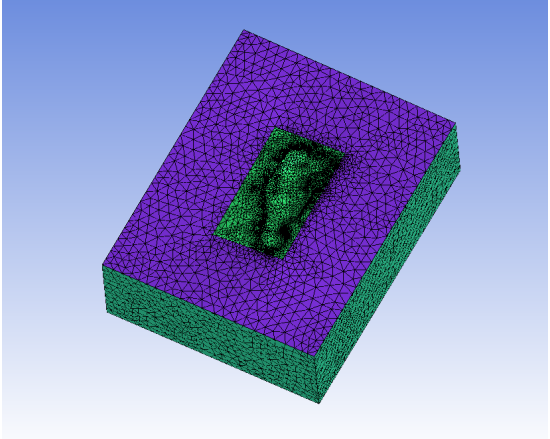
7.2 The cavity model

As explained in chapter 5, a requirement for the scanner equipment was to produce output which further could be analysed in FEA-based software. Models with corresponding surface as the degraded chain links, which could produce field output like displacements, stress and strains, were desired. In this section the process for creating a model based on a single cavity, consisting of volume elements, is presented. This model, from now on referred to as the cavity model, was used in a sub-modelling routine, which is presented in chapter 8. The modelling process consisted of several steps and is summarised in table 7.1. Table F.1 and F.2 provide more detailed information of the process.

A suitable cavity was extracted from the surface model explained in section 7.1 with the aid of GS14. This was done by erasing all polygons, except for the ones within a rectangular area surrounding the cavity. Of the original 1.64 million polygons in the surface model, around 21 000 triangles were kept intact. This resulted in a rough surface mesh with uneven edges as illustrated in figure 7.4, from now one referred to as the initial top surface model. The cavity model was intended to be shaped as a block with volume elements, where the initial top surface model constituted one of the sides. For this to be possible, some post-processing was necessary. The four sides needed to be approximately straight, and the complexity of the surface needed to be reduced, in order to limit the required volume elements in the final model.

In order to represent one cavity only, the area around the main cavity was straightened and rid of minor cavities and other rough areas. A smoothing process with minimum curvature prioritisation was carried out on this surface. The edges were straightened, resulting in four straight areas approximately perpendicular to each other, with the main cavity in the centre. Also the main cavity was smoothed in order to avoid sharp corners and edges, which could lead to stress singularities during numerical modelling. This was done with maximum prioritisation of the curvature. Finally some repair work was carried out by the aid of the function *Meshdoctor*. The resulting surface model, from now on referred to as the top surface model, is illustrated in figure 7.5. The top surface model consisted of around 23 000 elements and covered an area of approximately 145 mm².

Table 7.1: Modelling process for the 3D model.

Geomagic Studio 2014	Processing of the selected cavity	
↓	Creation of top surface	
ANSYS-ICEM CFD 17.0	Build solid model from top surface	
	Mesh model	

After being post-processed in GS14, the top surface model was imported in .stl format to the software [ANSYS ICEM CFD 17.0](#), from now on referred to as [ICEM](#). The modelling functions in ICEM enables the user to define walls around a surface geometry such as the top surface model. In this way a closed and hollow box was created, where the top surface model constituted one of the six sides. This box was to be meshed with volume elements. In order to declare the volume to be meshed, a so called "body point" was created within the hollow box.

4-node tetrahedral elements, in Abaqus named [C3D4](#), were used to mesh the cavity model in ICEM. The *Octree (Robust)* meshing method was utilised, with proximity based refinement. The refinement allows for a fine mesh in areas with complex geometry, and coarser mesh in areas with simple geometry. To avoid sharp edges which could cause singularities in the stress response, smoothing was enabled during the mesh routine. This was done with the *Smooth Mesh Globally* function with the criterion set to *quality*. Six mesh densities were used on the cavity model as described in table [E.3](#).

The maximum and minimum element size could be determined for each model, along with the edge criterion. This criterion is contributing when determining how fine a surface is meshed with tetrahedral elements. The value specifies how much of tetra edges that is allowed to stick outside of a surface. With low values comes a fine surface mesh (ANSYS ICEM CFD, Help System, Release 17.0). The prescribed values resulted in 48000 elements in the model with the coarsest mesh and 145000 elements in the model with the finest.

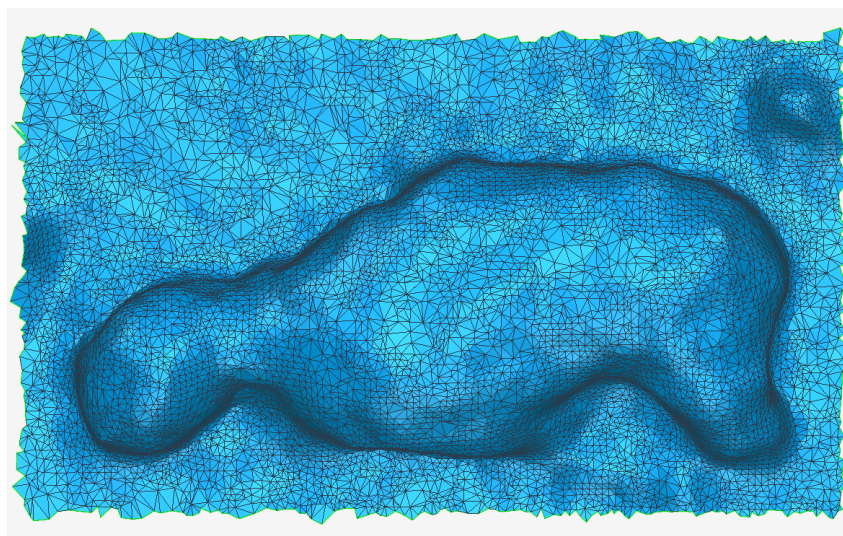


Figure 7.4: *The initial top surface model, extracted from the surface model.*

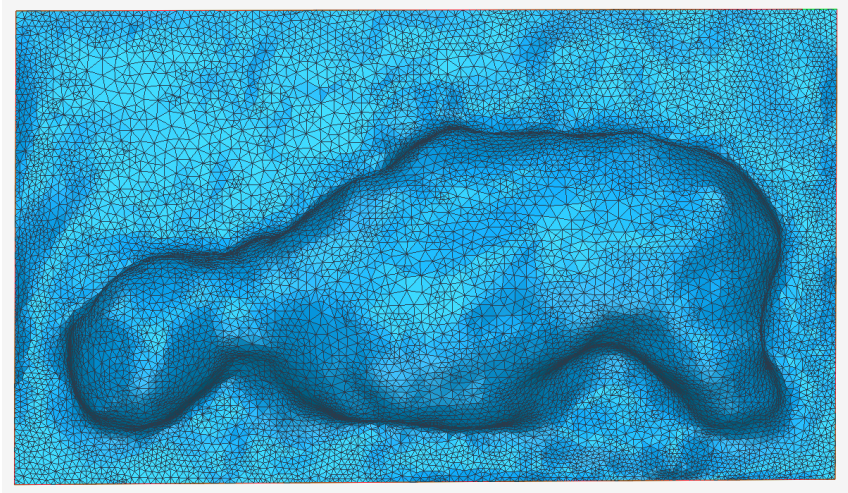


Figure 7.5: The final top surface model.

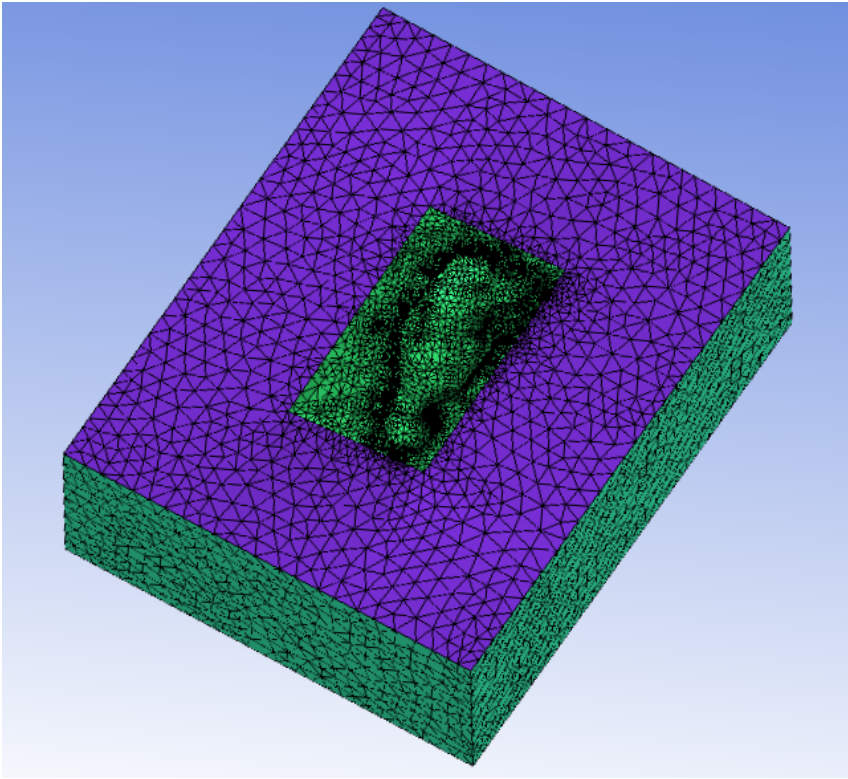


Figure 7.6: The cavity model with the finest mesh density used.

SUBMODELING IN ABAQUS

In this chapter, a stress analysis of a chain link with a single surface cavity is presented. This was done in Abaqus by using the cavity model, described in section 7.2, as a submodel. The submodeling routine presented is meant to illustrate a procedure for fatigue life analysis based on surface conditions, with accompanying possibilities and limitations. In future work with the project, the procedure could be used to analyse worst case scenarios of surface conditions of chain links, in terms of size, orientation and localisation of corrosion pits. Also interactions of multiple cavities could be analysed, without extensive requirements for computational time and resources.

8.1 Sub modelling

To obtain satisfactorily results in a model with complex geometry, a fine mesh is usually required. A model of a chain link with corrosion pits on the surface for instance, would require a mesh with high density close to the surface. Due to the complex and irregular geometry of cavities caused by corrosion, a full scale 3D model of a chain link would require a great amount of elements, which again would require an unacceptably high amount of computer resources. Even if the model only represented a minor part of a chain link, such as the CLS in figure 6.4 and 6.5, the costs of the required computational time could surpass the value of the results.

Submodeling enables thorough analysis of a specified local region in a large model, by using results from the large model as boundary conditions for a so called submodel. A submodel is an independent model from a specified location in the global model, usually meshed with a higher density of elements. By using the calculated displacements in the global model as specified boundary conditions for the submodel, accurate results may be obtained in the area of interest.

8.2 The global model

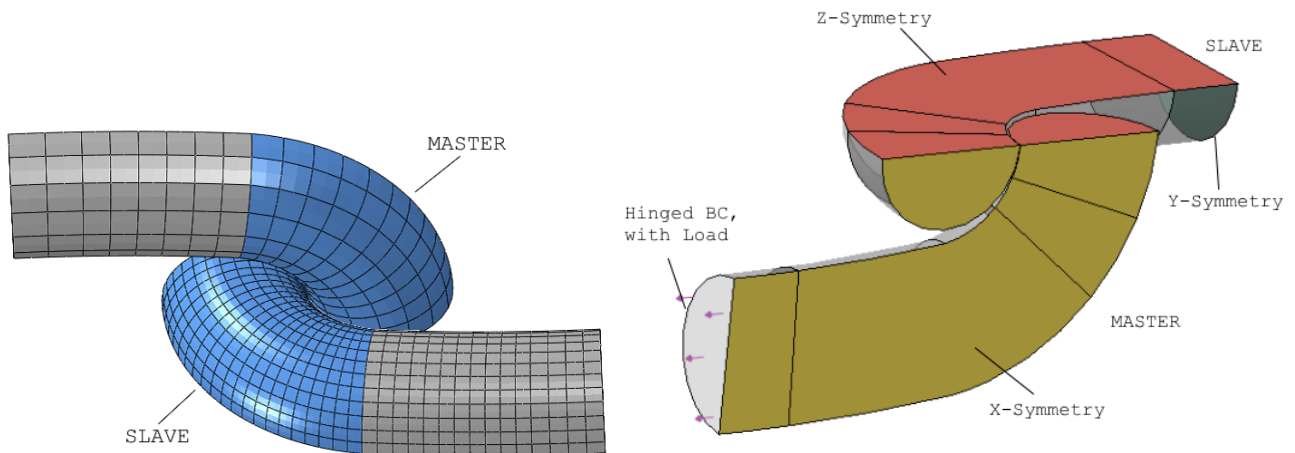


Figure 8.1: The master- and slave surface of the two chain links (Hove, 2016, p.46).

Figure 8.2: Loading and boundary conditions. The surface traction is illustrated with purple arrows (Hove, 2016, p.47).

The same model as presented in the thesis work of Hove (2016) was used as a global model in this analysis. Two chain links in contact under static tensile loading was modelled to produce the displacement field and stress response in a chain link. A short description of the modelling procedure follows. For more detailed description of the analysis, the reader is referred to (Hove, 2016, p.45).

Two chain links with a surface-to-surface interaction were modelled. One link was meshed coarsely and assigned a master surface, while the other was assigned a finer meshed slave surface. This is illustrated in figure 8.1. The purpose of the master link was to provide contact forces on the slave link, while the slave link was to provide the displacement field and stress response. 20-node hexahedral elements with quadratic interpolated displacement fields, in Abaqus named **C3D20**, were used. The links were modelled with a diameter of 76 mm and a geometry which followed the guidelines provided in (IACS, 2011, W22). Due to the three symmetry planes in a chain link, each link was modelled as a 1/8 part of full size. Figure 8.2 shows the boundary conditions in the global model, along with the surface traction on the master link. This surface was assigned a hinged boundary condition and loaded with a constant, uniform surface traction of 60 MPa. This ensured the master link movement as in the case with pure tensile loading. The analysis was carried out with linear elastic and homogeneous material behaviour, with a Young's Modulus value of 210000 MPa, a Poisson's Ratio of 0.29 and a mass density of 7850 kgm^{-3} .

8.3 The submodel

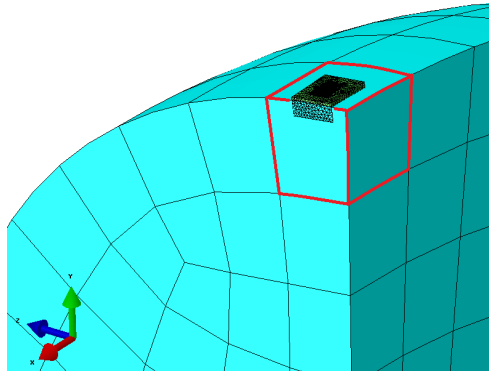


Figure 8.3: Positioning of the cavity model within C3D20 element nr 1509. The element 1509 is highlighted with red borders.

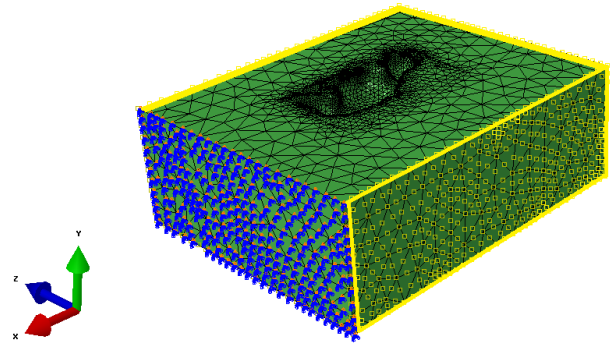


Figure 8.4: Boundary conditions for the cavity model. Blue markers indicates X-symmetry. Areas with yellow borders and squares read values from the global model.

The displacement field that was to be imposed as boundary conditions on the submodel, could be sampled from any part of the slave link in the global model. As explained in section 4.5, both the work at DSE and the work of Fredheim et al. (2013) showed a trend where failure initiated in the crown of the tested links. For this reason, the submodel was placed in the corresponding region of the slave link. In order to fit within one single C3D20 element, the C3D20 element number 1509, the model was scaled down. This is illustrated in figure 8.3. The resulting dimensions and location of the submodel is given in figure 8.5, table 8.1 and table 8.2.

Figure 8.4 illustrates the boundary conditions for the submodel. One side was assigned a x-symmetry boundary condition, in accordance with the boundary condition on the corresponding side of the slave link surface. The side with the cavity was modelled as a free surface with no boundary conditions. The four remaining sides were assigned submodel boundary conditions, where values were read from the corresponding area in the global model, in this case element number 1509. The setup simulated a scenario where five of the sides in the cavity model was "submerged" in the slave link volume.

The C3D4 elements in the cavity model was upgraded to 10-node quadratic tetrahedral elements, in order to increase the interpolation order and hence the quality of the results. The elements used in the analysis, are in Abaqus named C3D10. To evaluate convergence, six analysis were carried out with increasing mesh density in the submodel, in accordance

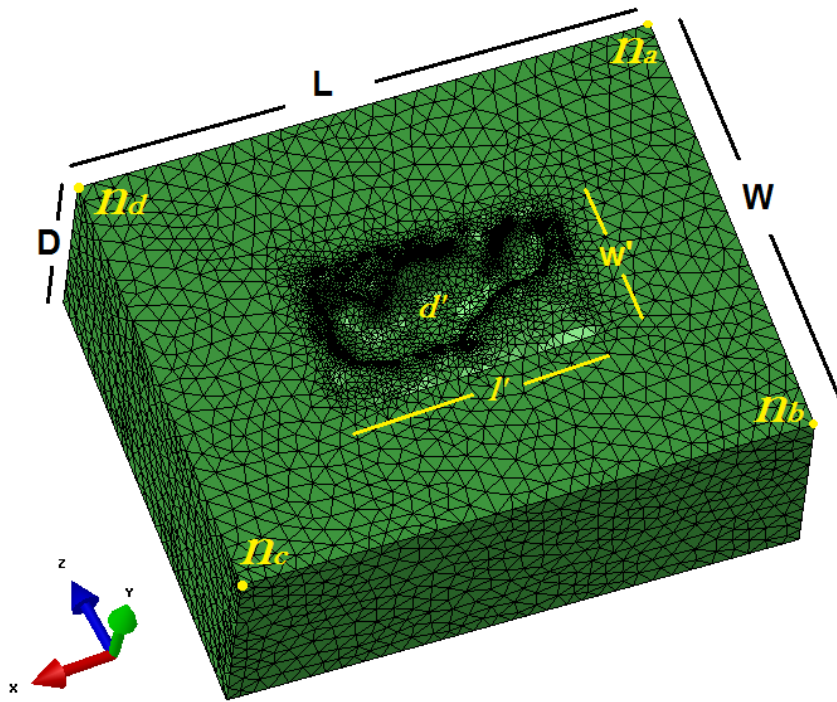


Figure 8.5: The resulting dimensions after downscaling the submodel.

Table 8.1: Dimension values of the downscaled submodel.

L [mm]	W [mm]	D [mm]	l' [mm]	w' [mm]	$\Delta d'$ [mm]
4.44	3.57	1.5	2.04	1.18	0.3-0.4

Table 8.2: Nodal point coordinates of the downscaled submodel.

n_a	n_b	n_c	n_d
-4.448, 75.318, 5.088	-4.442, 75.597, 1.528	0.000, 75.500, 1.500	-0.001, 75.177, 5.051

with table E3. In every analysis, the boundary conditions imposed on the submodel was sampled from the same single analysis of the global model. Except for the increasing mesh densities, all conditions were kept constant.

8.4 Results

8.4.1 The global model

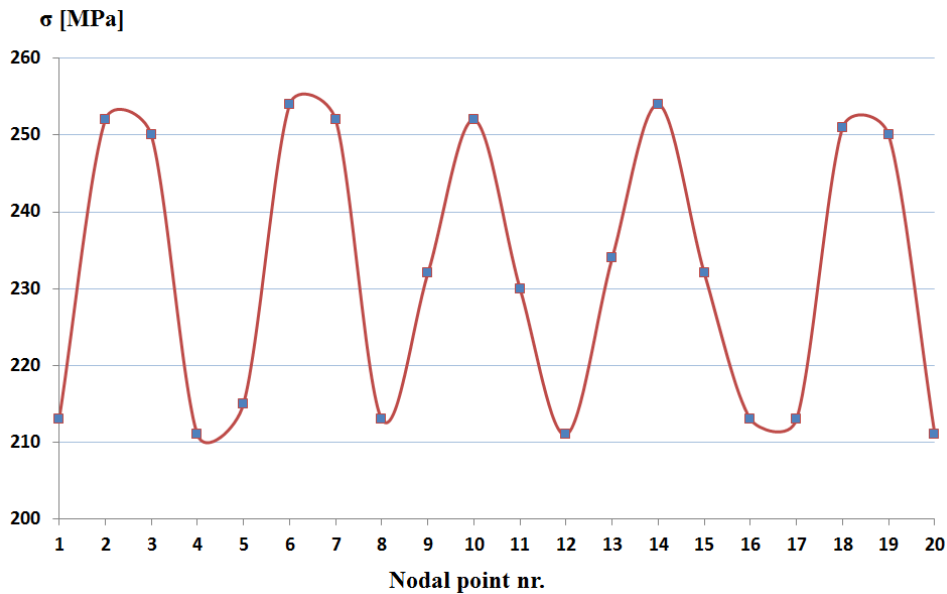


Figure 8.6: The maximum principal stresses in C3D10 element nr. 1509, sampled in the nodal points. The represented stress variation between each point is only illustrative and not representative for the exact response.

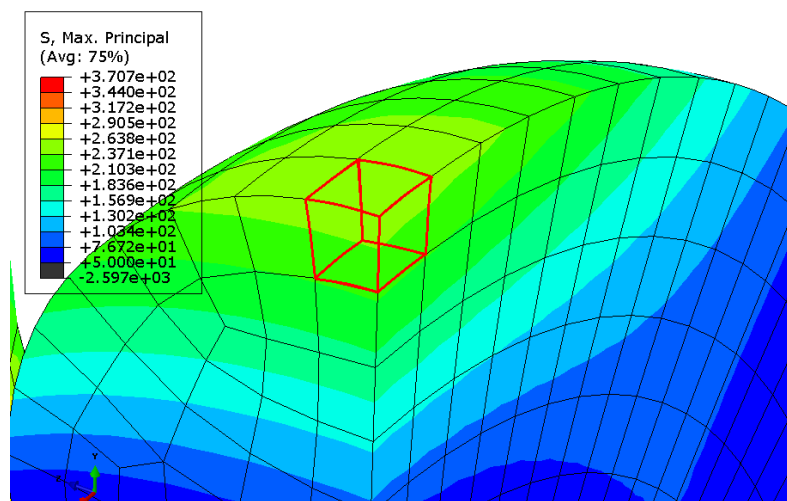


Figure 8.7: Maximum principal stresses in the global model. Element nr. 1509 is highlighted.

A relatively uniform stress distribution was found in the crown area of the slave link. This is illustrated in figure 8.7, represented with maximum principle stresses. The maximum and the minimum values of 370.7 MPa and -2597 MPa are located in the contact area between the master and the slave surface, and is hence not of interest. The maximum principle stresses in C3D20 element number 1509 is presented in figure 8.6, sampled at the nodes. Also here a rather uniform distribution could be observed with a minimum value of 211 MPa and a maximum of 254 MPa.

8.4.2 The submodel

The stress response in analysis 1 and 6 are illustrated in figure 8.8 and 8.9 respectively. As the figures indicate, a good conformity between each analysis could be observed regarding the distributed stress response. The response on the surface close to the edges was, as expected, close to the values in element nr 1509. For both analysis 1 and 6 the stresses on the surface varied between approximately 175 MPa to 285 MPa. This corresponds to deviations of approximately 17 % from the minimum-, and 12 % from the maximum value found in element number 1509. A trend could be observed where the stress near the constrained edge (x-symmetry) was higher than compared with the areas close to the edge on the opposite side of the cavity.

Good conformity could also be found regarding the location of the highest stress values. For every analysis, the highest stress values were found in two valleys within the cavity. The location of the maximum value could be found in the same area in every analysis, as illustrated in figure 8.10. This area will from now on be referred to as the critical area.

For the convergence study, the maximum value of the maximum principle stresses were sampled in each analysis. These values can be found in table 8.3, along with mesh details for every analysis.

Table 8.3: *Maximum Principle Stress in the cavity model analysis.*

Analysis nr	Max. element size	Min. element size	Edge criterion	Total nr. elements	Max. Princ. σ [MPa]
1	2.0	0.10	0.20	48 065	733.4
2	1.5	0.08	0.20	63 633	731.0
3	1.5	0.08	0.10	77 168	791.4
4	1.2	0.06	0.01	95 933	736.3
5	1.2	0.05	0.01	108 708	731.1
6	1.0	0.03	0.01	145 026	750.8

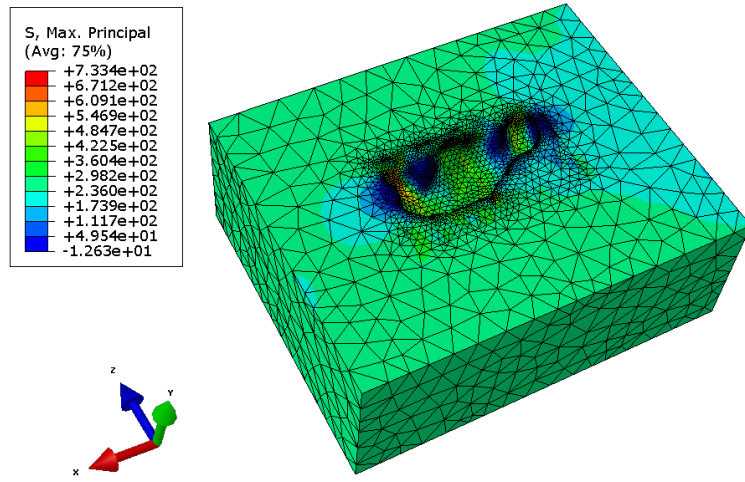


Figure 8.8: Stress response in submodel analysis nr. 1.

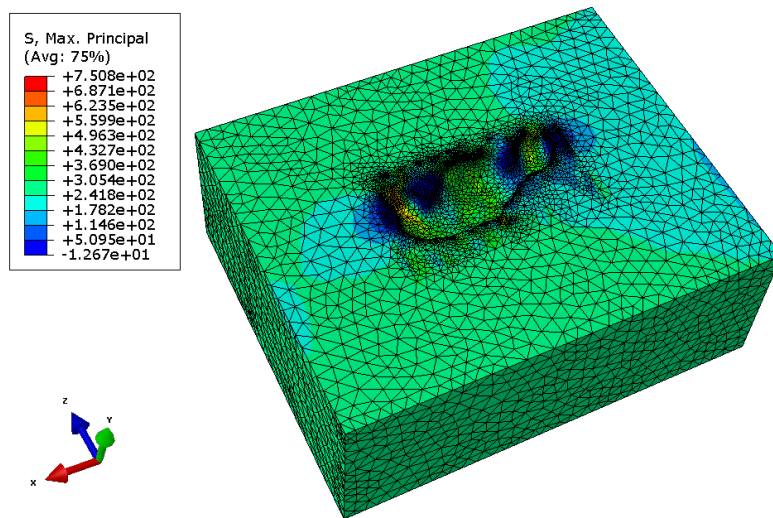


Figure 8.9: Stress response in submodel analysis nr. 6.

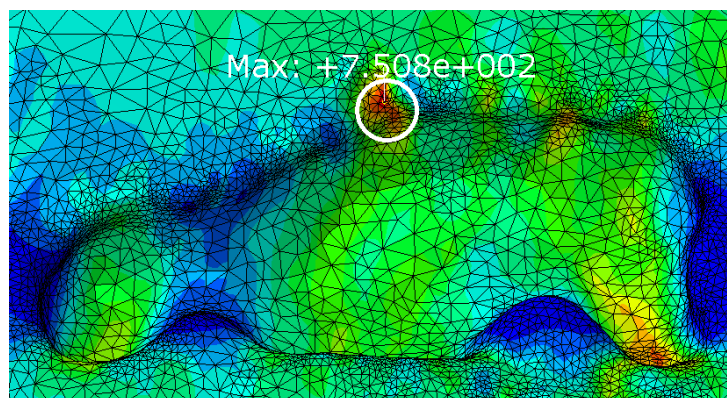


Figure 8.10: Area with the the highest values of stresses, here represented with the submodel in analysis nr. 6.

8.5 Discussion

Normally, both the solution in the global model and the submodel need to be evaluated regarding convergence. As the aim of this analysis was to highlight the submodeling procedure, limited attention was paid the global model. The stress response in the slave link was assumed stable, with a converged solution.

The conformity of the surface values in the six submodeling analyses, indicates a convergence of the solution for the areas close to the edges of the box. It is reasonable to believe that the maximum element size of 2.0, used in analysis 1, is adequate and that no further refinement of the areas along the edges is required.

The deviations between the surface stresses in the submodel analysis and the values obtained in C3D20 element number 1509 in the global analysis, could possibly be explained with the placement of the submodel inside one single C3D20 element. The displacements inside element number 1509 are interpolated from the nodal values. This means that the displacements, and hence the stresses, inside the element are not as accurate as in the nodal values. The surface values of the submodel are caused by the displacement field within element 1509. When comparing the surface values in the submodel with the nodal values of element 1509, some deviations should be expected. An other explanation for the deviations could be the box shaped geometry of the submodel. A displacement field develops differently in a curved shaped geometry like element number 1509, than in a cube. Since the deviations are limited, it was concluded that proper boundary conditions were imposed on the submodel and that the submodeling routine worked as intended.

Figure 8.11 illustrates how the maximum value of the maximum principle stress develops for each refinement of the mesh. As clearly illustrated, no convergence could be shown for the maximum value. As explain in section 3.3, the solution should decline steadily before approaching a certain value, as demonstrated in figure 3.7. The solution seems to oscillate around a value of approximately 750 MPa, with something which resembles to an outlier in analysis 3.

When examining the models, geometric deviations between the submodels were observed in the critical area. During meshing in ICEM, smoothing of the mesh was performed, in order to avoid sharp edges that could lead to stress singularities. When smoothing in ICEM, a function called *Freeze* may be enabled for certain elements. In this case, the nodes for

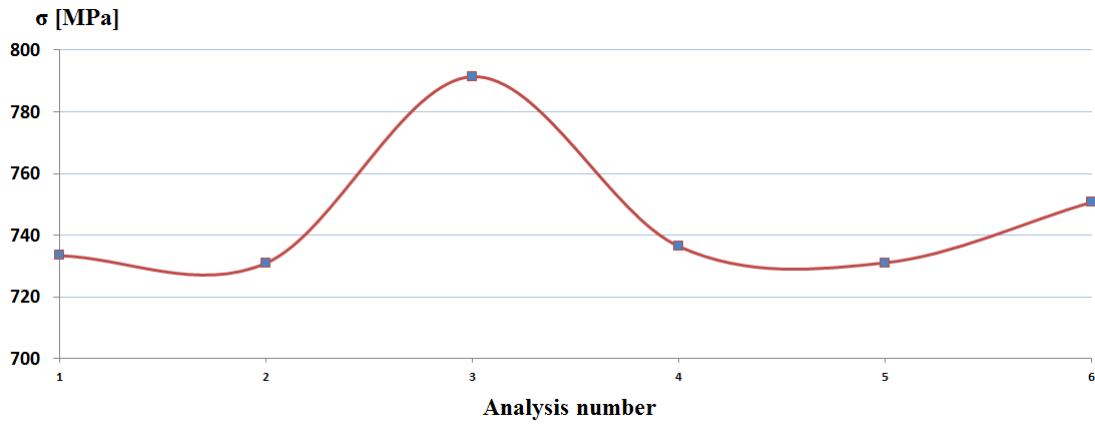


Figure 8.11: Variation of the maximum Principle Stress in the cavity model analysis.

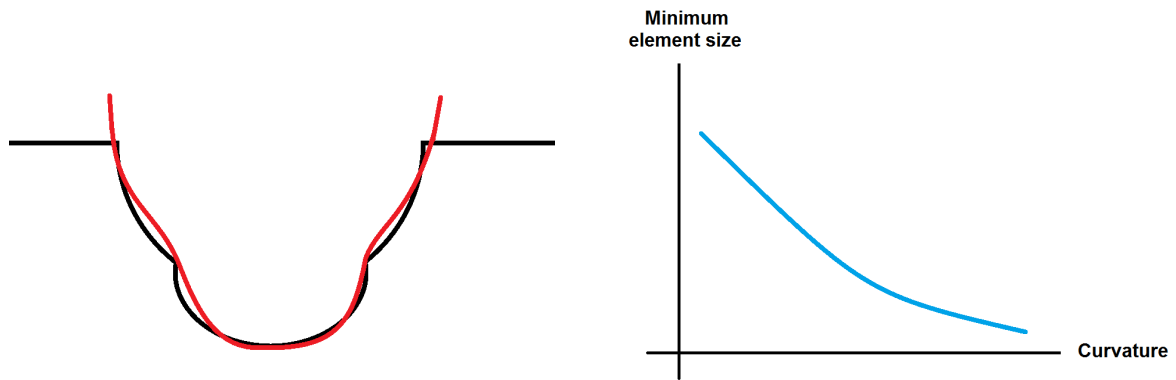


Figure 8.12: Fitting curves to CAD models in order to evaluate the curvature.

Figure 8.13: A hypothetical relation between the curvature of cavities and the required minimum element size.

these elements are fixed during smoothing (ANSYS ICEM CFD, Help System, Release 17.0). This was not done during the modelling procedure. It is therefore considered reasonable to believe that the location of the nodes shifted during smoothing. If this is the case, the different models did not mesh the critical area with the same nodal points and geometry. Even if a model was meshed finer than in a preceding analysis, the difference in the geometry could have resulted in higher stress values.

In order to adequately assess the results of a submodeling analysis as presented, a convergence study is required. A different mesh design where smoothing is avoided in the critical areas is recommended. A very fine mesh should be employed in these areas, to avoid stress singularities. Values for the minimum and maximum size of elements, and the required value for the edge criterion should be found.

A possible method for evaluating one of these parameters, for instance the minimum size of elements, could be to establish a relation with the curvature. Figure 8.12 and 8.13 illustrates the method. One could model different cavity geometries in Abaqus with simple load cases. By succeeding analyses for the same geometry, with increasing mesh density for each analysis, a tolerable error could be defined and the required mesh density could be stated for the particular geometry. The curvature of the analysed geometries could easily be described with the aid of splines. By carrying out multiple analyses on geometries with different curvatures, an empirical relation could be established where the required minimum size is given as a function of the curvature. When this relation is stated, one can evaluate the curvature of cavities like the one in the cavity model from section 7.2. The empirical relation would then give an estimate of the required minimum size of the mesh.

If smaller deviations between the areas close to the edges in the submodel and the corresponding area in the global model is desired, a simple convergence study regarding the mesh density in the global model could be carried out. A refinement of the area in close proximity of element number 1509 only, should be sufficient. Also a simple study could be carried out to find the ideal shape for the submodel. In this case, the same procedure as explained in section 8.2 and 8.3 could be carried out for different designs of the submodel. It is then suggested that the designs should follow the curved side of the chain link surface.

Finally, a study of the required size of the submodel should be carried out. Simple tensile analysis could be carried out on cavity models with decreasing depth, width and length. The

stress response on the surfaces without a cavity should be sampled. These areas should not be affected by the cavity, and have values close to the nominal values of a box without a cavity. If this is the case, the dimensions of the submodel is sufficient, and it can be used for submodeling analysis.

8.6 Possibilities and limitations

A major advantage of sub modelling considering this project, is that the same global model could be used for several analysis with different surface conditions. The chain model presented in section 8.2 could provide boundary conditions for as many submodels as desired. The cavity model could be scaled to different sizes, rotated to different orientations, placed in different areas of the slave link and so on. Several submodels based on different cavities could be made in the same way as described in section 7.2. In this way, worst case scenarios may be analysed.

Fatigue life may be estimated by combining the maximum principal stresses found with for instance the hot spot method. The theory of critical distances is also applicable with the maximum principal stresses.

The process with modelling and numerical analysis, as described in chapter 7 and 8, are rather comprehensive and time consuming. The process could be accelerated with the aid of scripting. If the requirements considering the model are known, the procedure could be automated and a substantial amount of time could be saved.

CONCLUDING REMARKS

In this thesis, mooring line failure has been investigated with respect to governing regulations and associated risks. The development on the [NCS](#) during the last 20 years has been illustrated through statistical data. Equipment for 3D representations have been evaluated through a feasibility study carried out at [NTNU](#). A scanner based on a combination of photogrammetry and structured light technology has been used to measure corroded chain surfaces. The output was post processed in *Geomagic Studio 14* and *ANSYS ICEM CFD* in order to create a surface model and a model consisting of volume elements. A submodel analysis has been carried out in Abaqus to simulate the effect of a single cavity on the surface of a chain link in tension.

In the following, the most important results and conclusions from the thesis work is summarised.

Mooring failure

Today's governing regulations states that flotel and production facilities should tolerate loss of two lines without serious consequences. Mobile drilling facilities should tolerate one.

Worrying trends regarding mooring line failure was reported by [PSA](#) for two periods. A frequency of failure on the [NCS](#) in the period 1996-2005, corresponded to one failure for every ten facility years. Between 2010 and 2014, a total of 16 line failures were reported.

Both the corrosion fatigue testing at [KT](#) and the test program presented by Fredheim et al. (2013), suggested that failure was most likely to happen in the crown region of common studless mooring chain links in tension.

The feasibility study

Of the evaluated equipment and software at NTNU, the *ATOS III* sensor at the [KT](#) was considered the best available option for this thesis work.

The use of photography in combination with photogrammetric software in inspection routines was highlighted as a possible valuable method for this project, provided a skilled photographer and adequate quality of the camera. Licenses for two suitable software, *AGISOFT*

PhotoScan and *Photomodeller Scanner*, was localised at the [IDI](#) and the [BAT](#).

A possibility for arranging an agreement with [Hexagon Manufacturing Intelligence](#) in order to borrow their highly accurate handheld scanner was found.

Experimental study

Best practice during measurement with the *ATOS III* sensor has been investigated. The procedure has been demonstrated to the personnel in the laboratory at [KT](#), in order to build competence at the [KT](#) and to aid in future work with this project.

Untreated, corroded, matte coloured surface has been found to give best measuring results. Treatment with developer spray, in order to produce a matte, light surface, has been proven redundant. Dark and bright regions on the same surface area to be measured, have been found undesirable as this resulted in lack of measuring points. The same unwanted effect was found when the corrosion layer had been scratched away, exposing shiny metal underneath.

Successful 3D measurements have been carried out of a [Chain Link Specimen](#) with corroded surface, using the *ATOS III* sensor. The results were exported in .stl format for further post processing.

Modelling

The measuring results from *ATOS III* have been reduced in size with almost 60%, in order to create a surface model with no mesh defects. The efficiency in handling the model was increased substantially.

A model representing a cavity on the [CLS](#) surface, fully compatible with FEA-based software, has been created.

Submodelling

The results along the sides of the submodel was comparable with the corresponding area in the global model. The conclusion was drawn, that proper boundary conditions were imposed on the submodel and that the submodeling routine worked as intended.

Conformity in the stress response close to the edges in the submodel was proven. It was concluded that the maximum size of 2.0 for the biggest elements resulted in an adequate solution of these areas, and that further reduction of this parameter was considered redundant.

The critical region in the submodel was found by sampling the maximum principal stress. The location was found to be located in the same region for all six analyses. Convergence of the maximum value for the maximum principal stress was not proven. The solution of the maximum value seemed to oscillate during refinement of the mesh. The smoothing routine in [ICEM](#) was suggested as the most likely cause for this behaviour. Suggestions were proposed for further convergence study, where the critical region was meshed fine, without the use of smoothing.

To relate the curvature of cavity geometries with the required minimum sizes for the smallest elements, was proposed as a method for evaluating convergence in further submodeling analysis.

Succeeding submodel analyses by using the same global model for collecting boundary conditions was highlighted as a method for analysing worst case scenarios. The position, orientation, size and number of cavities could be varied. By scripting the procedure, a wide range of scenarios could be simulated at minimum computer costs.

Submodel analysis

A convergence study for the submodel as explained in section 8.5 could be carried out. Smoothing should be avoided in the critical area, and the required size and shape of the model could be evaluated. To effectively evaluate convergence in future models, the relationship between curvature and required minimum size of the elements could be found as explained in the same section.

Inspection

Inspection routines were investigated in GS14. Dimensions like depth, width, volume and area could easily be drawn out of both single cavities and for the whole surface model. However, due to time limitations this work had to be cancelled. Further study on inspection routines should be carried out. Also methods for verification should be investigated. The equipment listed in chapter G has been considered as good options for doing more precise measurements than obtained with the *ATOS III* sensor. The measurements from such equipment could be considered as to give the "correct" values. By comparing results from *ATOS III* with these, the accuracy could be estimated.

BIBLIOGRAPHY

- Agisoft (2015). *Photoscan: Fully automated professional photogrammetric kit*, Promotional presentation, St. Petersburg, Russia. Available at http://www.agisoft.com/pdf/photoscan_presentation.pdf. Accessed: 24 May 2016.
- Ahmad, Z. (2006). *Principles of corrosion engineering and corrosion control*, Butterworth-Heinemann.
- Almar-Næss, A. (2009). *Avsmeltesveising*, Available at: <https://snl.no/avsmeltesveising>. Accessed: 10 June 2016.
- ANSYS ICEM CFD, Help System (Release 17.0). *Global Mesh Setup*, Ansys, Inc. Accessed: 10 July 2016.
- Artec3D (2016). *Professional 3D scanning solutions*, Promotional brochure. Available at <http://www.artec3d.com/files/pdf/ArtecScanners-Booklet-EURO.pdf>. Accessed: 24 May 2016.
- ASTM International (2005). *Standard Guide for Examination and Evaluation of Pitting Corrosion, Standard ASTM G46-94*, ASTM International West Conshohocken, PA.
- ASTM International (2013). *Standard Terminology Relating to Fatigue and Fracture Testing, Standard ASTM E1823 13*, ASTM International West Conshohocken, PA.
- Bache, T. B. (2016). *3D scanning of a corroded chain link*. Project Thesis, The Norwegian University of Science and Technology.
- Bjørnsen, E. (2014). *Chains in mooring systems*, Master's thesis, Norwegian University of Science and Technology, Trondheim, Norway.
- Cook, R. D. et al. (2002). *Concepts and applications of finite element analysis*, fourth edn, John Wiley & Sons.
- Det Norske Veritas (2007). *Accident Statistics for Floating Offshore Units on the UK Continental Shelf 1980-2001, Research report RR567*, Health and Safety Executive (HSE), Norway.

- DNV GL (2015). *Offshore mooring chain, Standard DNVGL OS-E302*, DNV GL AS.
- Dowling, N. E. (2013). *Mechanical Behaviour of Materials: Engineering Methods for Deformation, Fracture, and Fatigue*, 4 edn, Pearson Education Limited, England.
- Eos Systems Inc (2016). *How accurate is PhotoModeler?*, Available at: http://info.photomodeler.com/blog/kb/how_accurate_is_photomodeler/. Accessed: 26 May 2016.
- Faltinsen, O. M. (1990). *Sea loads on ships and offshore structures*, Cambridge ocean technology series, Cambridge University Press, Cambridge, UK.
- Fredheim, S., Reinholdtsen, S., Håskoll, L. and Lie, H. (2013). 'Corrosion Fatigue Testing of Used, Studless, Offshore Mooring Chain', *32nd International Conference on Ocean, Offshore and Arctic Engineering*, number 10609 in *OMAE 2013*, Nantes, France.
- Geomagic Support Center (2016a). *How to convert a point object to a polygon object using wrap*, Instructional video. Available at: <http://support1.geomagic.com/Support/5605/5668/en-us/Article/View/1412/How-to-Convert-a-Point-Object-to-a-Polygon-Object-using-Wrap>. Accessed: 25 May 2016.
- Geomagic Support Center (2016b). *How to Reduce Noise*, Instructional video. Available at: <http://support1.geomagic.com/Support/5605/5668/Article/View/1461/How-To-Reduce-Noise>. Accessed: 26 May 2016.
- Gom mbH (2008). *ATOS V6.1 - Software User Manual*. Atos_v61_1st_en_rev-b, 7-Jul-2008.
- Gom mbH (2010). *ATOS V7 - Hardware User Manual*. Atos3_rev01_v7_en_rev-b, 12-Oct-2010.
- Hagland, J. (2015). *Alexander L. Kielland Ulykken*, Online dictionary. Article available at: https://snl.no/Alexander_L._Kielland-ulykken. Accessed: 10 May 2016.
- Hexagon Metrology (2015). *Leica Absolute Traker AT960*, Promotional brochure. Available at <http://hexagonmi.com/products/3d-laser-scanners/leica-tscan-5>. Accessed: 24 May 2016.

- Hoel, A., Hove, M. and Tømmervåg, K. H. (2015). *Assessment of the life of offshore mooring chains*. Project thesis, The Norwegian University of Science and Technology.
- Hove, M. (2016). *Growth of fatigue cracks in mooring line chains*, Master's thesis, Norwegian University of Science and Technology, Trondheim.
- Howell, G., Duggal, A. and Lever, G. (2001). 'The Terra Nova FPSO Turret Mooring System', *Offshore Technology Conference*, number 13020 in *Annual Offshore Technology Conference, OTC*, Offshore Technology Conference, Houston, U.S.A.
- IACS (2011). *Offshore Mooring Chain, Standard W22*, International Association of Classification Societies.
- Konica Minolta (2006). *Non-contact 3D digitizer VIVID 910/VI-910*, Konica Minolta. Instructional Manual (Hardware).
- Kvitrud, A. and Bache, B. T. (2014). *Anchor line failures Norwegian continental shelf 2010-2014, Report 992081*, Petroleumstilsynet.
- Kvitrud, A. and Vinnem, J. E. (2006). *Forankring av innretninger på norsk sokkel, Report Ptil-05-07*, Petroleumstilsynet.
- Mack, R., Gruy, R. and Hall, R. (1995). 'Turret Moorings for Extreme Design Conditions', *Offshore Technology Conference*, number 7696 in *Annual Offshore Technology Conference, OTC*, Offshore Technology Conference, Houston, U.S.A., pp. 23–31.
- Mathisen, K. M. (2015). *The Finite Element Method Introduction and Fundamental Concepts*. Lecture Notes for Course TKT4192, Finite Element Methods in Strength Analysis, Norwegian University of Science and Technology.
- McKeown, R., Bisset, A. and McKeown, S. J. (2011). 'Offshore Replacement Of A Damaged FPSO Fairlead', *SPE Offshore Europe Oil and Gas Conference and Exhibition*, number SPE-145190-MS in *SPE Offshore Europe 2011*, Society of Petroleum Engineers, Aberdeen, UK.
- Moe, P. T. (2006). *Report on the study of optical measurement systems 2005-2006, Report*, SINTEF (The Norwegian University of Science and Technology).

- Morandini, C. and Legerstee, F. (2009). 'Consistent Integrity of Mooring System', *The Nineteenth International Offshore and Polar Engineering Conference*, International Society of Offshore and Polar Engineers (ISOPE, Osaka, Japan, pp. 625–632.
- Noble Denton Europe Limited (2006). *Floating production system JIP FPS mooring integrity, Research report 444*, Health and Safety Executive (HSE), Aberdeen, UK.
- Norsk Standard (2011). *Metallic materials - Charpy pendulum impact test - Part 1: Test method, Standard ISO 148-1:2010*, Norsk Standard.
- Norwegian Broadcasting Corporation (2015). *Lekter slet seg i Nordsjøen*, Online video. Available at: www.nrk.no/nyheter/lekter-slet-seg-i-nordsjoen-1.12727478. Accessed: 12 May 2016.
- Norwegian Maritime Authority (2009). *Forskrift om posisjonerings- og ankringsystemer på flyttbare innretninger (ankringsforskriften 09)*, Available at: https://lovdata.no/dokument/SF/forskrift/2009-07-10-998#KAPITTEL_3. Accessed: 23 June 2016.
- Petroleum Safety Authority Norway (2015). *Regulations relating to design and outfitting of facilities, etc. In the petroleum activities (the facilities regulations)*, Available at: http://www.ptil.no/innretningsforskriften/category380.html#_Toc438215277. Accessed: 23 June 2016.
- Petroleum Safety Authority Norway (2016a). *Regulations relating to health, safety and the environment in the petroleum activities and at certain onshore facilities (the framework regulations)*, Available at: http://www.ptil.no/rammeforskriften/category381.html#_Toc440873984. Accessed: 23 June 2016.
- Petroleum Safety Authority Norway (2016b). *RNNP: Hovedrapport Sokkel, Report*, Petroleumstilsynet, Stavanger, Norway. Available at: <http://www.ptil.no/hovedrapport-sokkel/category1230.html>. Accessed: 12 May 2016.
- Petroleum Safety Authority Norway (2016c). *RNNP: Sammendragsrapport Sokkel, Report*, Petroleumstilsynet, Stavanger, Norway. Available at <http://www.ptil.no/sammendragsrapport-sokkel/category1229.html> Accessed: 12 May 2016.

- Petroleum Safety Authority Norway (2016d). *Role and area of responsibility*, Available at: <http://www.psa.no/role-and-area-of-responsibility/category916.html>. Accessed: 12 May 2016.
- Petroleum Safety Authority Norway (2016e). *Trends in risk level in the petroleum activity (RNNP)*, Available at: <http://www.psa.no/about-rnnp/category911.html>. Accessed: 12 May 2016.
- Petroleum Safety Authority Norway (2016f). *Trends in Risk Level in the Petroleum Activity. Summary Report 2015, Report*, Petroleumstilsynet, Stavanger, Norway. Available at <http://www.psa.no/summary-report-2015/category1194.html> Accessed: 12 May 2016.
- Ramnäs Bruk (2015). *Ramnäs Bruk Product Catalogue*, Product Catalog, Ramnäs, Sweden. Available at: <http://ramnas.com/downloads/>. Accessed: 20 June 2016.
- Ramnäs Bruk (2016). *Shackles*, Available at: <http://ramnas.com/products/shackles/>. Accessed: 16 June 2016.
- Schuman-Olsen, H., Skotheim, O., Breivik, G. M. and Johansen, G. (2010). *Sensors and environmental study - Next Generation Robotics for Norwegian Industry (NextGenRob), Report*, SINTEF.
- ShapeCrafter (2016a). *About ShapeCrafter 3D*, Available at: <http://www.shapecrafter.no>. Accessed: 24 May 2016.
- ShapeCrafter (2016b). *ShapeCrafter fact sheet*, Promotional article. Available at: <http://www.shapecrafter.no>. Accessed: 24 May 2016.
- ShapeCrafter (2016c). *The world's most accurate real-time 3D RGBD camera*, Promotional article. Available at: <https://vr2.verticalresponse.com/s/shapecrafternews>. Accessed: 13 July 2016.
- Stachowiak, G. W. and Batchelor, A. W. (2006). *Engineering Tribology (Third Edition)*, third edn, Butterworth-Heinemann.
- Statoil worldwide: Norway (2013). Available at: <http://www.statoil.com/en/about/worldwide/norway/>. Accessed: 6 May 2016.

- Tømmervåg, K. (2016). *Degradation mechanisms of offshore mooring lines*, Master's thesis, Norwegian University of Science and Technology, Trondheim.
- Vinnem, J. E. (2001). *Operational safety of FPSOs: Initial summary report, Research report 2000/086*, Norwegian University of Science and Technology, Norway. Prepared for the Health and Safety Executive (HSE).

3D REPRESENTATION AT NTNU

Table A.1: Available equipment at NTNU for making 3D representations.

ATOS III SO	<i>GOM mbH</i>
Principle	Structured-Light and photogrammetry
User Field	Car industry, quality control, reverse engineering +++
Accuracy	0.03-0.08 mm
Output	STL, PLY, POL, C3D, G3D, ASCII, +++
URL	http://gom.com/ http://www.cascade.se/sv-se/hem
Location	Laboratory at the KT , Richard Birkelands vei 1A
Contact person	Odd Kristian Nerdahl, odd.nerdahl@ntnu.no
Used because	Adequate accuracy, availability, low costs
Shapecrafter 3D	<i>Shapecrafter 3D</i>
Principle	Structured-light Triangulation
User Field	In-line inspection, 3D machine vision, 3D part localization +++
Accuracy	50 μ m
Resolution	Lateral: 1920 x 1200 (2.3 Mpixels), Depth: 1/10.000 of image width
Output	Point cloud w/ RGB in the form of a 1920x 1200 matrix of (X,Y,Z) and RGB values (Binary or ASCII format)
URL	http://www.shapecrafter.no/
Location	Richard Birkelands vei 2B
Contact person	Øystein Skotheim, info@shapecrafter.no
Why not used	Lack of automatic merging function
ARTEC Eva	<i>Artec 3D</i>
Principle	Structured-Light Triangulation
User Field	Automotive industry, architecture, heritage preservation +++
3D Point Accuracy	0.1 mm
Output	OBJ, PLY, WRL, STL, AOP, ASCII, PTX, E57, XYZRGB
URL	https://www.artec3d.com/hardware/artec-eva
Location	IDI , Sem Sælandsvei 9
Contact person	Theoharis Theoharis , theotheo@idi.ntnu.no
Why not used	Accuracy, lack of assistance

Agisoft Photoscan	<i>Agisoft LLC (Software)</i>
Principle	Photogrammetry
User Field	Topography, archaeology, art and design +++
Accuracy	Up to 3 cm for aerial-, up to 1 mm for close-range photography
Output	OBJ, PLY, U3D, PDF, Agisoft OC3, XYZ text file format +++
URL	http://www.agisoft.com/
License holder	BAT , Høgskoleringen 7A
Contact person	Knut Ragnar Holm , knut.r.holm@ntnu.no
Why not used	Accuracy, lack of experienced personnel (photography)
PhotoModeller Scanner	<i>Eos Systems Inc (Software)</i>
Principle	Photogrammetry
User Field	Geology, mining, civil engineering, surveying, architecture +++
Accuracy	1 part in 25000 when using coded targets
Output	3DS, OBJ, STL, DXF, 3dm, igs, txt +++
URL	http://www.photomodeler.com/index.html
License holder	IDI , Sem Sælandsvei 9
Contact person	Torbjørn Hallgren, torbh@idi.ntnu.no
Why not used	Lack of experienced personnel (photography)
Vivid 910	<i>Konica Minolta</i>
Principle	Laser triangulation
User Field	Rapid prototyping, cultural heritage, medical +++
Accuracy	≈ 0.22 mm, depending on lens-set and measuring conditions
Output	WRL, STL, HRC, OBJ, DXF, ASC, MGF, WRL
URL	konicaminolta.com/instruments/download/instruction_manual/3d
Location	BAT , Høgskoleringen 7A
Contact person	Knut Ragnar Holm , knut.r.holm@ntnu.no
Why not used	Accuracy, imperfect merging function
Leica T-Scan AT901	<i>Hexagon Manufacturing Intelligence</i>
Principle	Flying dot technology
User Field	Automotive industry, reversed engineering, aircraft +++
Accuracy	+/- 50 μm
Output	STL +++ (depending on applied software)
URL	http://hexagonmi.com/products/3d-laser-scanners/leica-tscan-5
Location	Not available at the time of writing
Contact person	Knut Sørby, knut.sorby@ntnu.no
Comment	Leica T-Scan is compatible with 6-7 software, e.g. Spatial Analyzer
Why not used	Availability, limited time

SHAPECRAFTER 3D

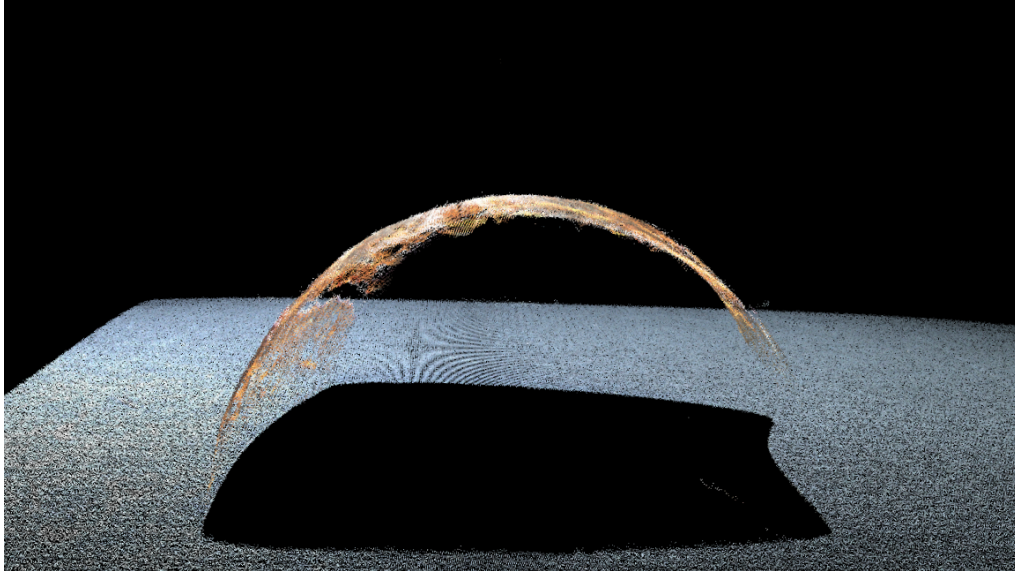


Figure B.1: Measurement result of the *Chain Link Specimen (CLS)* using Shapecrafter 3D. Results presented with CloudViewer.

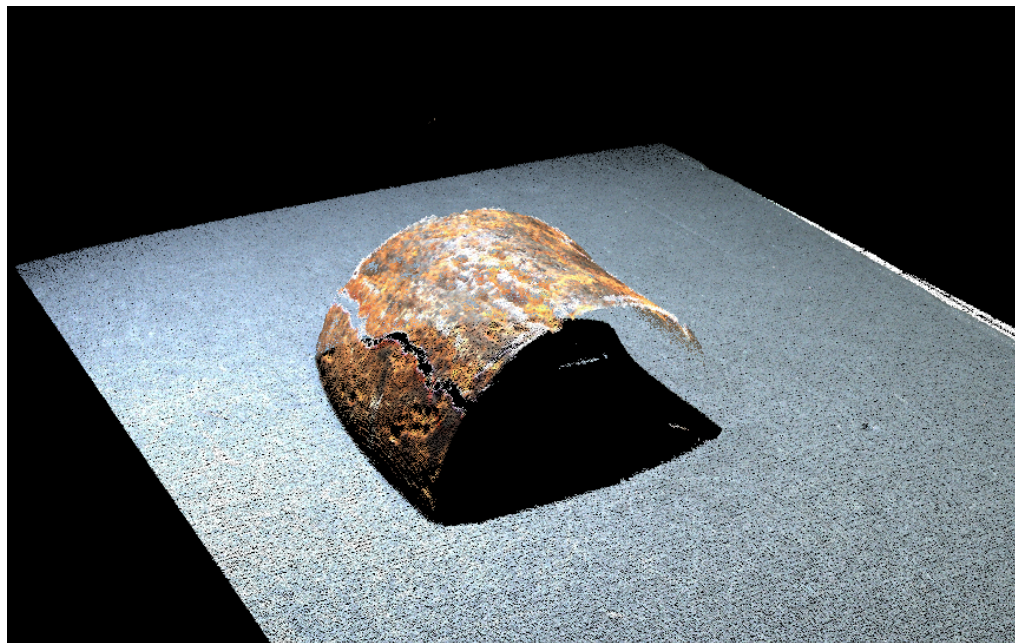



Figure B.2: Measurement result presented with CloudViewer. The transparent "border" along the side corresponds to a white labelling line on the CLS. If very dark and very bright regions are present in the image simultaneously, it can be difficult to adjust the iris and exposure time of the camera to ensure a good results in the entire measurement area. The latest version of ShapeCrafter 3D (due to be released in Q4, 2016) has implemented various High Dynamic Range modes which significantly improve the results in these kinds of situations.



Generated with [Agisoft PhotoScan](#)

Figure C.1: 3D model of chain link specimen, made with Agisoft Photoscan.

Figure C.1 illustrates a snapshot of the 3D model made with Agisoft Photoscan from ten photos of the CLS. The photos were taken with a low quality, 16-megapixel, *Samsung Galaxy S5 neo* mobile camera. Better quality is to be expected with better quality of the utilised camera. The circular markers on the surface are reference points originating from measurement with ATOS III SO and should not be mistaken for coded targets compatible with photogrammetric software. In the 3D pdf file, the model may be examined by zooming, rotating etc. The 3D pdf file, with full 3D properties, may be accessed in the digital version of this thesis by following the link: 

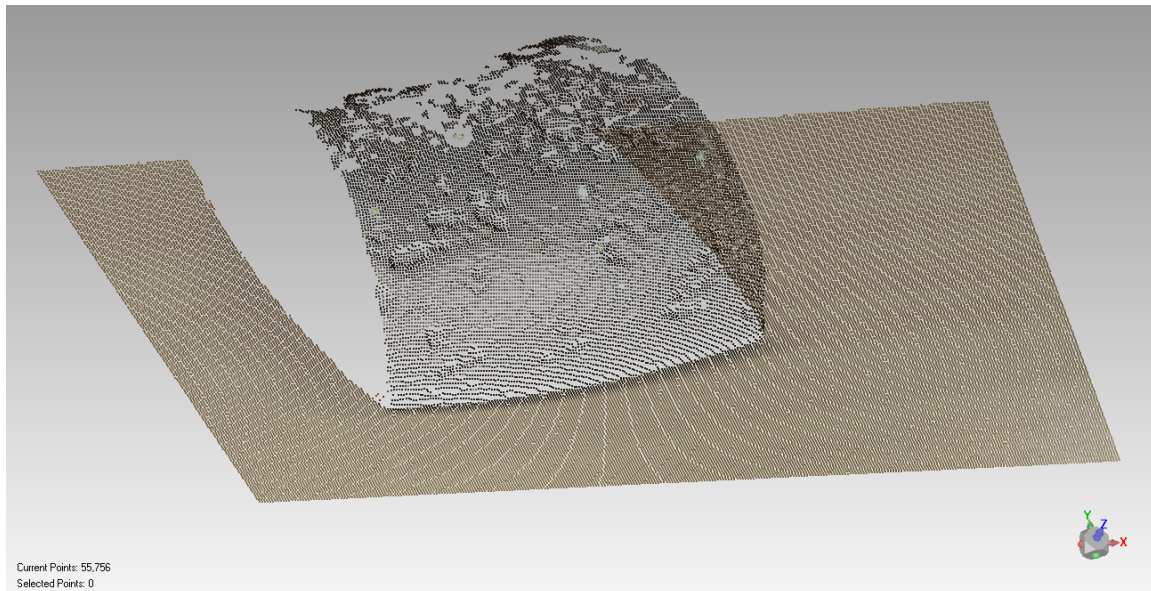


Figure D.1: Resulting point cloud from measurement of the CLS with the Konica Minolta 3D Digitizer. Results treated and presented with Geomagic Studio 2014.

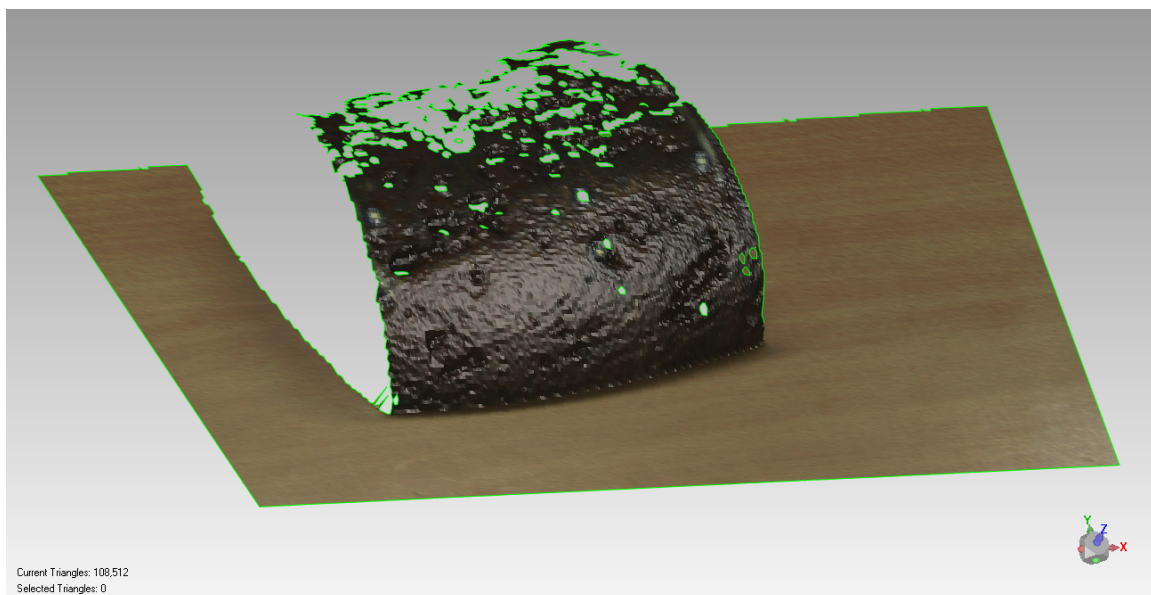


Figure D.2: The polygon mesh based on the point cloud, in .vvd format. Results treated and presented with Geomagic Studio 2014.

THE SURFACE MODEL

The surface model was made by post-processing the ISM in GS14 and is described in section 7.1. Table E.1 summarise the procedure, where the first operation is presented in the top and the last in the bottom.

Table E.1: Making the surface model in GS14.

Operation	Job description	Model information
<i>Importing file</i>	Importing ISM in .stl format	Polygon mesh <ul style="list-style-type: none"> • 4053675 polygons • 15476 mm²
<i>Point Cloud conversion</i>	Conversion from polygons to points	Point cloud <ul style="list-style-type: none"> • 2154118 points
<i>Point clean-up</i>	Erasing outliers and disconnected components: <ul style="list-style-type: none"> • Sensitivity: 85 %, Separation: low, Size: 5 Reduction of noise <ul style="list-style-type: none"> • Free-form shapes, smoothness level: 1 • Deviation limit: 0.3041 mm, Iterations: 1 Sampling: <ul style="list-style-type: none"> • By curvature, 75 % 	Point cloud <ul style="list-style-type: none"> • 1391364 points
<i>Wrapping</i>	Creation of polygon mesh <ul style="list-style-type: none"> • Keep original data, erase small components • Max triangles: 1.7 million, prioritise quality 	Polygon mesh <ul style="list-style-type: none"> • 1699999 polygons
<i>Meshdoctor</i>	Repairing of mesh <ul style="list-style-type: none"> • Self-intersections, tunnels, spikes • Highly creased edges 	Polygon mesh <ul style="list-style-type: none"> • 1698746 polygons
<i>Manual cutting</i>	Removal of areas of insufficient quality <ul style="list-style-type: none"> • Manual selection 	Polygon mesh <ul style="list-style-type: none"> • 1639635 polygons
<i>Hole filling</i>	Fill single <ul style="list-style-type: none"> • Manual selection and modifications 	Polygon mesh <ul style="list-style-type: none"> • 1640566 polygons
<i>Meshdoctor</i>	Repairing of mesh <ul style="list-style-type: none"> • Spikes 	Polygon mesh <ul style="list-style-type: none"> • 1640566 polygons • 12313 mm²

THE CAVITY MODEL

The cavity model was made by post-processing the surface model as described in section 7.2. Table F1 summarise the procedure for creating the top surface model in GS14. Table F2 describe the modelling process carried out in ICEM in order to model a closed, hollow box using the top surface model. The different mesh densities used to mesh the hollow box, is described in table F3.

Table F.1: *Creating the top surface in GS14.*

Operation	Job description	Mesh information
<i>Open file</i>	Open the surface model	<ul style="list-style-type: none"> • 1 640 566 polygons • 12 313 mm²
<i>Erasing components</i>	Erasing polygons and points that are not associated with the selected cavity	<ul style="list-style-type: none"> • 20 649 polygons
<i>Defeature</i>	Removing minor cavities from the area surrounding the selected cavity	<ul style="list-style-type: none"> • 20 423 polygons
<i>Modify boundaries</i>	Straightening of four surrounding boundaries	<ul style="list-style-type: none"> • 20 423 polygons
<i>Remeshing</i>	Remesh along new boundaries <ul style="list-style-type: none"> • Repairing areas with self-intersecting elements 	<ul style="list-style-type: none"> • 22 903 polygons
<i>Smoothing</i>	Smoothing area around the cavity <ul style="list-style-type: none"> • Max smoothness level, max strength • Min curvature priority Smoothing area containing the cavity <ul style="list-style-type: none"> • Max smoothness level, medium strength • Max curvature priority 	<ul style="list-style-type: none"> • 22 903 polygons
<i>Mesh doctor</i>	Smoothing spikes	<ul style="list-style-type: none"> • 22 903 polygons • 145.3 mm²

Table F.2: Modelling the cavity model in ICEM.

Operation	Job description	Model information
<i>Import file</i>	Import top surface in .stl format	Geometry components: • Surface
<i>Create box</i>	Extract curves from surfaces: • Faceted, Angle for surface: 85 Create points: • Angle for curves: 30, Base Point and Delta Create curves: • By angle: 85, Segment curve	Geometry components: • Surface, lines and points
<i>Create Body</i>	Material point: • Centroid of two points	Geometry component: • Body
<i>Create walls</i>	Create/ Modify surface: • From 2-4 curves, tolerance 0.0	Geometry components: • Surfaces
<i>Define parts</i>	Assign geometry to parts	Parts
<i>Repair geometry</i>	Build Diagnostic Topology: • Tolerance: 0.0	

Table F.3: Different mesh specifications used on the cavity model.

Model nr	Max. element size	Min. element size	Edge criterion	Total nr. elements
1	2.0	0.10	0.20	48065
2	1.5	0.08	0.20	63633
3	1.5	0.08	0.10	77168
4	1.2	0.06	0.01	95933
5	1.2	0.05	0.01	108708
6	1.0	0.03	0.01	145026

EQUIPMENT FOR VERIFICATION PURPOSES

Table G.1: Equipment which potentially could be used for verification purposes.

HG-C1030	<i>Panasonic</i>
Type	Micro Laser Distance Sensor
Description	Mounted on a rig and controlled with a step motor system
Accuracy	10 μm (Repeatability)
Measurement range	± 5 mm (Vertical)
URL	www.panasonic-electric-works.com/eu/hg-c-measurement-sensor.htm
Location	Laboratory at the KT , Richard Birkelands vei 1A
Contact person	Odd Kristian Nerdahl, odd.nerdahl@ntnu.no
Comment	Limitations regarding dimensions of the object to be measured
InfiniteFocus	<i>Alicona</i>
Type	Optical 3D microscope
Description	Six objectives with varying magnification (2.5x-100x)
Accuracy	10 nm-2.3 μm (Vertical resolution)
Measurement range	0.16 mm-5.63 mm (Lateral)
URL	https://www.ntnu.edu/ipm/tribology-lab/ifm http://www.alicon.com/products/infinitefocus/
Location	Tribology lab at IPM , Richard Birkelandsvei 2B
Contact	https://www.ntnu.edu/ipm/tribology-lab
Comment	Resolution and measurement range depends on the utilised objective